NAVAL POSTGRADUATE SCHOOL

MONTEREY, CALIFORNIA

THESIS

TURNING VANES IN EXHAUST DUCT FLOW: STUDY FOR ENERGY EFFICIENCY, OPTIMIZATION AND PRESSURE DROP MITIGATION

by

Mark A. Beale

September 2014

Thesis Advisor: Sanjeev B. Sathe
Co-Advisor: Knox T. Millsaps

THIS PAGE INTENTIONALLY LEFT BLANK

REPORT DOCUMENTATION PAGE

Form Approved OMB No. 0704–0188

1. AGENCY USE ONLY *(Leave blank)*	**2. REPORT DATE** September 2014	**3. REPORT TYPE AND DATES COVERED** Master's Thesis

4. TITLE AND SUBTITLE
TURNING VANES IN EXHAUST DUCT FLOW: STUDY FOR ENERGY EFFICIENCY, OPTIMIZATION AND PRESSURE DROP MITIGATION

5. FUNDING NUMBERS

6. AUTHOR(S) Mark A. Beale

7. PERFORMING ORGANIZATION NAME(S) AND ADDRESS(ES)
Naval Postgraduate School
Monterey, CA 93943–5000

8. PERFORMING ORGANIZATION REPORT NUMBER

9. SPONSORING /MONITORING AGENCY NAME(S) AND ADDRESS(ES)
N/A

10. SPONSORING/MONITORING AGENCY REPORT NUMBER

11. SUPPLEMENTARY NOTES The views expressed in this thesis are those of the author and do not reflect the official policy or position of the Department of Defense or the U.S. Government. IRB Protocol number ____N/A____.

12a. DISTRIBUTION / AVAILABILITY STATEMENT
Approved for public release; distribution is unlimited

12b. DISTRIBUTION CODE

13. ABSTRACT (maximum 200 words)

This thesis presents a computational fluid dynamics (CFD) study on the effects of turning vanes and their placement in an exhaust duct with a sharp bend of ninety degrees and the application toward waste heat recovery devices.

CFD models were implemented in ANSYS/CFX to handle flow in both laminar and turbulent regimes. Applying the principles from the Reynolds-averaging Navier-Stokes governing equations as well as the k-ε turbulent model, accurate simulations were performed to explore the behavior of exhaust gas flow field, pressure drops and recirculation zone sizes for various flow Reynolds (Re) numbers. The effects of turning vane location, vane setting angle, and number of vanes were evaluated. Flow visualization was used as a means of determining ideal locations for future installation of WHR devices.

Results for $5000<Re<2x10^5$ showed significant improvement in pressure drop across the 90-degree duct with a single turning vane, showing ranges of 50–70% reduction in overall pressure drop across the duct. This pressure reduction could yield significant fuel savings compared to an engine or generator without a turning vane. Increasing the number of vanes neither reduced the pressure drop further, nor did it reduce the size of the primary recirculation zone.

14. SUBJECT TERMS Turning Vane, 90-degree Bend, Pressure Drop, Waste Heat Recovery, 2D	**15. NUMBER OF PAGES** 81
	16. PRICE CODE

17. SECURITY CLASSIFICATION OF REPORT	**18. SECURITY CLASSIFICATION OF THIS PAGE**	**19. SECURITY CLASSIFICATION OF ABSTRACT**	**20. LIMITATION OF ABSTRACT**
Unclassified	Unclassified	Unclassified	UU

NSN 7540–01–280–5500

Standard Form 298 (Rev. 2–89)
Prescribed by ANSI Std. 239–18

THIS PAGE INTENTIONALLY LEFT BLANK

Approved for public release; distribution is unlimited

TURNING VANES IN EXHAUST DUCT FLOW: STUDY FOR ENERGY EFFICIENCY, OPTIMIZATION AND PRESSURE DROP MITIGATION

Mark A. Beale
Lieutenant, United States Navy
B.S., United States Naval Academy, 2008

Submitted in partial fulfillment of the
requirements for the degree of

MASTER OF SCIENCE IN MECHANICAL ENGINEERING

from the

NAVAL POSTGRADUATE SCHOOL
September 2014

Author: Mark A. Beale

Approved by: Sanjeev B. Sathe
Thesis Advisor

Knox T. Millsaps
Co-Advisor

Garth Hobson
Chair, Department of Mechanical and Aerospace Engineering

THIS PAGE INTENTIONALLY LEFT BLANK

ABSTRACT

This thesis presents a computational fluid dynamics (CFD) study on the effects of turning vanes and their placement in an exhaust duct with a sharp bend of ninety degrees and the application toward waste heat recovery devices.

CFD models were implemented in ANSYS/CFX to handle flow in both laminar and turbulent regimes. Applying the principles from the Reynolds-averaging Navier-Stokes governing equations as well as the k-ε turbulent model, accurate simulations were performed to explore the behavior of exhaust gas flow field, pressure drops and recirculation zone sizes for various flow Reynolds (Re) numbers. The effects of turning vane location, vane setting angle, and number of vanes were evaluated. Flow visualization was used as a means of determining ideal locations for future installation of WHR devices.

Results for $5000<Re<2x10^5$ showed significant improvement in pressure drop across the 90-degree duct with a single turning vane, showing ranges of 50–70% reduction in overall pressure drop across the duct. This pressure reduction could yield significant fuel savings compared to an engine or generator without a turning vane. Increasing the number of vanes neither reduced the pressure drop further, nor did it reduce the size of the primary recirculation zone.

THIS PAGE INTENTIONALLY LEFT BLANK

TABLE OF CONTENTS

I. INTRODUCTION....1
A. MOTIVATION....1
B. BACKGROUND....2
C. LITERATURE SEARCH....4
D. PROBLEM STATEMENT....6
E. OBJECTIVES....8

II. GOVERNING EQUATIONS AND PARAMETERS....9
A. CONTINUITY....9
B. NAVIER-STOKES EQUATIONS....9
C. DERIVED EQUATIONS FOR MODEL VALIDATION AND NON-DIMENSIONAL PARAMETERS....10
1. Equations for Laminar Model Validation....10
2. Equations for Turbulent Model Validation....12
3. Non-dimensional Parameters....13
4. Non-dimensional Parameter Ranges for Navy and Marine Corps Systems....15

III. NON-DIMENSIONAL MODEL GEOMETRY....17

IV. LAMINAR MODEL VALIDATION....19
A. MESH SIZING....19
B. EVALUATION OF VALIDATION RESULTS....19

V. TURBULENT MODEL VALIDATION....23
A. MESH SIZING....23
B. ANSYS/CFX SET-UP....23
C. EVALUATION OF VALIDATION RESULTS....23

VI. DISCUSSION OF RESULTS....27
A. VELOCITY PLOT FOR NO TURNING VANE CASE....27
B. VELOCITY PLOT FOR ONE TURNING VANE CASE....29
C. EXIT VELOCITY PROFILE FOR OUTLET PORTION OF EXHAUST DUCT....30
D. VELOCITY PLOT FOR A TURNING VANE PLACED IN THE UPPER LEFT CORNER OF 90^{O} DUCT....32
E. PRESSURE CONTOUR FOR NO TURNING VANE CASE....33
F. PRESSURE CONTOUR FOR ONE TURNING VANE CASE....34
G. PRESSURE CONTOUR FOR ONE TURNING VANE PLACED IN THE UPPER LEFT CORNER OF A 90^{O} DUCT....35
H. EFFECT OF VARIOUS VANE CONFIGURATIONS ON PRESSURE DROP IN A 90^{O} EXHAUST DUCT BEND....37
1. Plotted Results for ΔP^{*}....38
2. Plotted Results for ΔP^{**}....43

3. Plotted Results for Recirculation Zone Size 46
VII. CONCLUSION 49
APPENDIX A. MODEL GEOMETRY 51
APPENDIX B. MODEL SETUP 53
APPENDIX C. VELOCITY VECTOR PROFILE PLOTS FOR A 90^{O} EXHAUST BEND 57
LIST OF REFERENCES 61
INITIAL DISTRIBUTION LIST 63

LIST OF FIGURES

Figure 1. Exhaust duct geometry with 90^o bend. 3
Figure 2. Exhaust duct geometry without a bend. 3
Figure 3. Energy recovery and pressure mitigation proposal from LT Mark Beale and Dr. Sanjeev Sathe to U.S. Marine Corps Expeditionary Energy Office (E2O) (from Sathe & Beale, 2013; Sathe & Millsaps, 2014) 7
Figure 4. NPS, U.S. Navy and U.S. Marine Corps Waste-Heat Recovery System Roadmap (from Sathe & Millsaps, 2014). 8
Figure 5. Schematic of flow through two parallel plates, showing laminar fully developed flow (from Anand, 2006). 11
Figure 6. Non-dimensional geometry of 90^o exhaust duct with one turning vane in XY plane. 17
Figure 7. Velocity developing profiles for laminar model validation runs. 20
Figure 8. Moody diagram showing plotted Darcy friction factor value lines, with point value data for CFD results (from Kiijarvi, 2001) 24
Figure 9. Non-dimensional velocity profile of 90^o bend without a turning vane for Re = 76,800, $D^* = 0.04$. 27
Figure 10. Non-dimensional velocity profile of 90^o bend with one turning vane for Re = 76,800, $D^* = 0.04$, $c^* = 0.35$, $r^* = 0.4$, $t^* = 0.07$. 29
Figure 11. Non-dimensional exit velocity profile for 90^o bend, showing effect on velocity profile near the bend for Re = 76,800, $D^* = 0.04$, $c^* = 0.35$, $r^* = 0.4$, $t^* = 0.07$. 30
Figure 12. Non-dimensional exit velocity profile for 90^o bend, showing effect on velocity profile far downstream for Re = 76,800, $D^* = 0.04$, $c^* = 0.35$, $r^* = 0.4$, $t^* = 0.07$. 31
Figure 13. Non-dimensional velocity profile of 90^o bend with one turning vane located near the upper left corner for Re = 76,800, $D^* = 0.04$, $c^* = 0.18$, $r^* = 0.2$, $t^* = 0.07$. 32
Figure 14. Non-dimensional pressure profile for 90^o bend without a turning vane for Re = 76,800, $D^* = 0.04$. 34
Figure 15. Non-dimensional pressure profile for 90^o bend with a turning vane for Re = 76,800, $D^* = 0.04$, $c^* = 0.35$, $r^* = 0.4$, $t^* = 0.07$. 35
Figure 16. Non-dimensional pressure profile for 90^o bend with a turning vane placed in upper left corner of duct bend for Re = 76,800, $D^* = 0.04$, $c^* = 0.18$, $r^* = 0.2$, $t^* = 0.07$. 36
Figure 17. Non-dimensional pressure drop values for ΔP^* in an exhaust duct with a 90^o bend. 38
Figure 18. Non-dimensional locations of pressure drop calculations for 90^o bend. 39
Figure 19. Profile view of one vane configuration for $D^* = 0.04$, $c^* = 0.35$, $r^* = 0.4$, $t^* = 0.07$. 40
Figure 20. Profile view of one vane rotated counter-clockwise from horizontal configuration for $D^* = 0.04$, $c^* = 0.35$, $r^* = 0.4$, $t^* = 0.07$. 40

Figure 21. Profile view of one vane placed in upper left corner of 90^o bend configuration for $D^* = 0.04$, $c^* = 0.18$, $r^* = 0.2$, $t^* = 0.07$. 41
Figure 22. Profile view of three smaller vane configuration for $D^* = 0.04$, $c^* = 0.18$, $r^* = 0.2$, $t^* = 0.07$. Note: Multiple small vanes have been used in rounded ducts. 41
Figure 23. Non-dimensional pressure drop values for ΔP^{**} in an exhaust duct with a 90^o bend for $D^* = 0.04$. 43
Figure 24. Non-dimensional recirculation zone size in an exhaust duct with 90^o bend for $D^* = 0.04$. 46
Figure 25. Non-dimensional primary recirculation zone size. 47
Figure 26. Non-dimensional velocity vectors in primary recirculation zone for Re = 76,800, $D^* = 0.04$, $c^* = 0.35$, $r^* = 0.4$, $t^* = 0.07$. 57
Figure 27. Non-dimensional velocity vectors in secondary recirculation zone for Re = 76,800, $D^* = 0.04$, $c^* = 0.35$, $r^* = 0.4$, $t^* = 0.07$. 58
Figure 28. Non-dimensional velocity vectors along turning vane for Re = 76,800, $D^* = 0.04$, $c^* = 0.35$, $r^* = 0.4$, $t^* = 0.07$. 59

LIST OF TABLES

Table 1. Range of non-dimensional parameter values for the Navy and Marine Corps systems. 15
Table 2. CFD Darcy friction factor calculations at varying Reynolds numbers. 24
Table 3. Non-dimensional pressure drop values and percentage reduction between single vane and no vane configurations. 42
Table 4. Non-dimensional pressure drop values and percentage reduction between a single vane in the upper left corner of the bend and no vane configurations. Refer to Figure 21 for geometry of 1 vane in upper left corner. 45
Table 5. Non-dimensional b^* values for various vane configurations for $D^* = 0.04$. 48

THIS PAGE INTENTIONALLY LEFT BLANK

LIST OF ACRONYMS AND ABBREVIATIONS

CFD	computational fluid dynamics
RANS	Reynolds-averaged Navier-Stokes
WHRS	waste-heat recovery system
E2O	USMC Expeditionary Energy Office
IR	Infrared
STP	standard temperature and pressure
CCW	counter-clockwise
CW	clockwise

THIS PAGE INTENTIONALLY LEFT BLANK

NOMENCLATURE

Symbols	Equation	Description	Units
A		Cross-sectional area	[m^2]
D_h	2D	Hydraulic diameter	[m]
f		Darcy friction factor	[1]
g		Acceleration due to gravity	[m/s^2]
h		Head loss	[m]
$\dot{m}$		Mass flow rate	[kg/s]
P		Pressure	[Pa]
R		Universal gas constant	[J/kg-K]
ρ		Density	[kg/m^3]
U		Inlet velocity	[m/s]
c		Chord line/length	[m]
ΔP*	$dP/\rho U^2$	Non-dimensional pressure drop	[1]
ΔP**	$dPD_h/\mu U$	Non-dimensional pressure drop	[1]
Re		Reynolds number	[1]
u*		Non-dimensional velocity	[1]
c*		Non-dimensional chord length	[1]
r*		Non-dimensional vane radius	[1]
t*		Non-dimensional vane thickness	[1]
k		Turbulence kinetic energy	[m^2/s^2]
ε		Turbulence eddy dissipation	[m^2/s^3]
u		Velocity in the x-direction	[m/s]
v		Velocity in the y-direction	[m/s]
w		Velocity in the z-direction	[m/s]
K_L		Major head loss coefficient	[1]

THIS PAGE INTENTIONALLY LEFT BLANK

I. INTRODUCTION

A. MOTIVATION

Most of the focus on overall engine efficiency concerns itself with the actual engine cycle. However, much is to be gained by researching and studying the effects of reducing backpressure on the engine by the exhaust gases. In many of today's Navy-Marine Corps engine designs, the exhaust duct or pipe design is constrained by a limited amount of space due to the complexity of ships and generators and their function-over-form design criteria, and therefore may have sharp bends.

Significant effort has been put into developing ways to harvest waste energy from combustion engines (Sathe & Beale, 2013). The most obvious and applicable area from which to harvest waste- heat energy is in the exhaust duct region. Arbitrary placement of a waste-heat recovery system (WHRS) may in the end be more detrimental to an operating engine system due to possible increases in back-pressure and could also result in an inefficient heat exchange due to placement of the system in a possible "dead" or recirculation zone in the exhaust gas flow (Sathe & Beale, 2013). To mitigate this, a study on duct bends of 90-degrees was necessary to properly evaluate the fluid flow in this regime and to properly assess and predicts its behavior and performance. The 90-degree geometry was chosen because it most accurately represented the geometry used in Navy and Marine Corps engine and generator systems currently in used. The introduction of a turning vane in the 90-degree bend was a means of reducing backpressure as well as a method for more accurately determining the most optimal location for WHRS placement.

An interesting phenomenon occurs in exhaust ducts with 90-degree elbows. In bends of 90-degrees or more, an eddy is formed in the corner and creates a recirculating flow that opposes the primary direction of the exhaust gases. In order to reduce the backpressure caused by recirculation zones and reduce soot accumulation. The eddy recirculation zones tend to accumulate soot, thereby increasing pressure drop. It is of interest to reduce the size of this zone. To further understand the recirculation zone

phenomenon, a study of the effects of various flow conditions in an exhaust ducts by varying flow conditions, vane orientation, quantity of vanes and vane placement was conducted.

B. BACKGROUND

The use of turning vanes in industry is not a new concept. The heating, venting and air conditioning industry uses turning vanes to redirect flow in 90-degree bends and in other applications to provide the most efficient means of cooling or heating a space. The use of turning vanes is used in gas-turbine engine design, and while they are called guide vanes they serve a similar purpose to those turning vanes used by the heating, venting and air-conditioning (HVAC) industry; redirect flow for optimal use. Keeping these two examples in mind, the purpose of installing one, or a series of, turning vane(s) in a 90-degree exhaust duct bend will serve two-fold: to reduce engine back-pressure and thus improve fuel economy, and to predict flow patterns in the outlet portion of the exhaust duct. This study focused on the optimal placement for a single turning vane within a 90^o bend.

The effect of an idealized placement of a turning vane within a sharp-cornered 90^o bend has not been studied (sharp corners occur in naval systems due to compartment restrictions). There is research into the effect of turning vanes on 90^o bends with rounded corners, as explained in Idelchik's *Handbook of Hydraulic Resistance* (Idelchik, 1994). Another area where research is lacking is into the effect of a turning vane on the recirculation zone size. Recirculation zones tend to accumulate soot and other particles, increase pressure drop as well as increase the frequency of required maintenance needed to reduce flow blockage. A connection can be made from the size of the recirculation zone to the life of the duct, time and money spent in maintenance on the exhaust duct, and the effectiveness of WHR devices downstream of the 90^o bend.

To evaluate the problem of backpressure in common USN/USMC generators and propulsion engines, Bernoulli's equation was applied to the initial problem. For a pipe with a single, 90-degree bend, the pressure drop across that pipe will be a known value larger than a pipe of the same length but continuous in its control volume (that is to say

without a 90-degree bend). Figure 1 shows the geometry of the case that I evaluated as a part of this thesis. Figure 2 shows a straight duct without any bends.

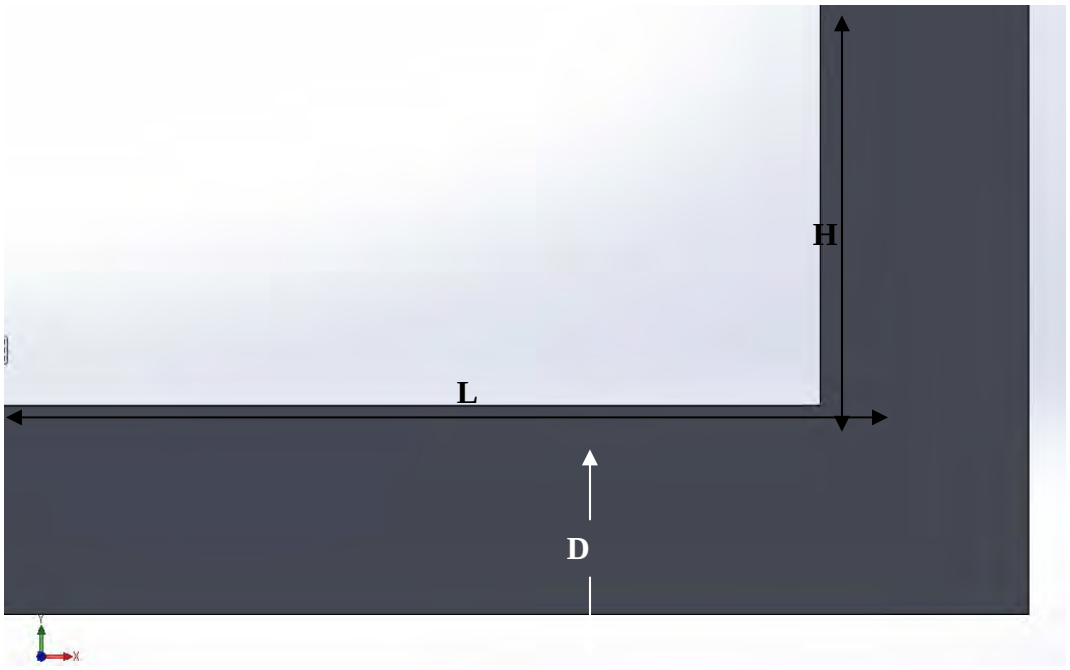

Figure 1. Exhaust duct geometry with 90^{o} bend.

Figure 2. Exhaust duct geometry without a bend.

Demonstrating why the pressure drop is higher in Figure 1 than in Figure 2, Bernoulli's equation was evaluated:

$$\frac{P_1}{\gamma}+\frac{V_1^2}{2g}+h_1=\frac{P_2}{\gamma}+\frac{V_2^2}{2g}+h_2. \quad (1)$$

For the straight pipe in Figure 2, $h_1 = h_2$ and therefore these terms cancel each other. For the 90-degree bend in Figure 1, $h_1 = 0$ and $h_2 = y_2$, where y_2 is some height above the reference plane. However, in the case of gases since the densities of the fluid are much smaller than the density of a liquid, the head loss (h) terms become negligible. To account for the increased pressure drop in a pipe with a sharp-angled bend, four key characteristics must be considered. First, there is a momentum change experienced by the flow when it changes direction by 90-degrees. Second, there is an increase in friction along the walls of the duct as the flow is forced to change directions. Third, there is a wake created by the flow particles as they go through the bend. Fourth and finally, the hydraulic diameter (D_h) of the pipe is effectively reduced by the creation of a recirculation zone in the duct bend. Thus, the case of Figure 1 will show an additional pressure drop term over the length of the duct compared to the duct in Figure 2 (Idelchik, 1994).

From the simple analysis of Bernoulli's equation and the application of the four characteristics described above it can be seen that pressure drop over a duct can become very large and ultimately affect the performance of an internal combustion engine. To further study the effects of pressure drop across the duct and the effects of a turning vane, I made use of computational fluid dynamics (CFD) software available at NPS.

C. LITERATURE SEARCH

Though vast amounts of resources have been put into developing ways to better improve engine efficiency and fuel economy on the front-end of the engine (air intake and the actual combustion cycle itself), the amount of resources for studying exhaust gas flow was smaller.

From the literature search conducted, the effect of turning vanes in sharp cornered ducts (as encountered in naval systems with size restrictions) has not been fully studied. Several cases have been studied for flow in ninety-degree bends; however, each of these cases studied flow in ninety degree bends with rounded corners. This thesis will study the effect of a ninety-degree bend with sharp, or non-rounded, corners. Also, the effect of turning vanes on the reduction of primary and secondary recirculation zones, which will affect soot and particle accumulation sites, has not been studied. Furthermore, from the research conducted there are not any studies that evaluate the flow field for a turning vane in a 90^o bend with the intent to optimize waste heat recovery device placement in an exhaust duct.

Most of the sources encountered were of great assistance in modeling turbulent flows and establishing the correct parameters needed to ensure that the models being run were accurate and did not require extraordinary computational time. The information that did refer to turning vane use consisted of recommended size and number of vanes, courtesy of I. E. Idelchik's *Handbook of Hydraulic Resistance* (Idelchik, 1994). From the knowledge gathered from this source optimal vane sizing was attained. Joshi and Sathe, in their parametric study on natural convection cooling, discussed numerical methods for a fluid regime (Sathe & Joshi, 1992). Hobson's lecture on turbulence modeling was greatly useful in establishing boundary conditions and overall problem set-up for evaluation using ANSYS/CFX software (Hobson, 2013). For model validation, Molki discusses the development of a fully developed laminar flow (Molki & et al, 2013), Anand discusses the fully developed flow for both laminar and turbulent models (Anand, 2006), and Kiijarvi provided methods for computing Darcy friction factors given various parameters to validate the turbulent model used (Kiijarvi, 2011). Modeling turbulent flow using the k-ε model, as discussed in Patankar's text, *The Turbulence-Kinetic-Energy Equation* (Patankar, 1980), was crucial in understanding the effects of turbulence in a simulated model.

These references provided a solid baseline from which the work outlined in this thesis was conducted. Specifically, the reduction of backpressure in an exhaust duct and its application to WHR devices was of major importance. As a result, new work was

conducted on studying the effect of vane placement within a duct, as well as a study on the effect of the turning vane on the recirculation zone size and potential implications on WHR device placement.

D. PROBLEM STATEMENT

The U.S. Marine Corps Expeditionary Energy Office (E2O), in partnership with the Naval Postgraduate School, has been conducting studies on the impact of WHR devices installed in diesel generator sets (GENSET) and has been looking for alternative solutions to reducing fuel costs while maintaining operational standards of current field generators. To effectively study the impact of WHR devices on current field GENSETs, as well as to find a means to reduce fuel consumption (and thus fuel cost) through backpressure reduction, an idea to install a vane inside the exhaust duct was proposed. By reducing backpressure up to 50% in some instances it would be possible to save between 3–5% fuel consumption; this would project to possibly millions of dollars a year in savings for the USMC and USN.

The idea of installing turning vanes into exhaust ducts inside of 90-degree bends was approved by E2O, and said research was funded accordingly for future improvements in the areas of energy recovery. The quad-chart proposal submitted by the author and thesis advisor, Dr. Sanjeev Sathe, is shown in Figure 3. The proposal considered altering various parameters to be examined and evaluated during the course of the work.

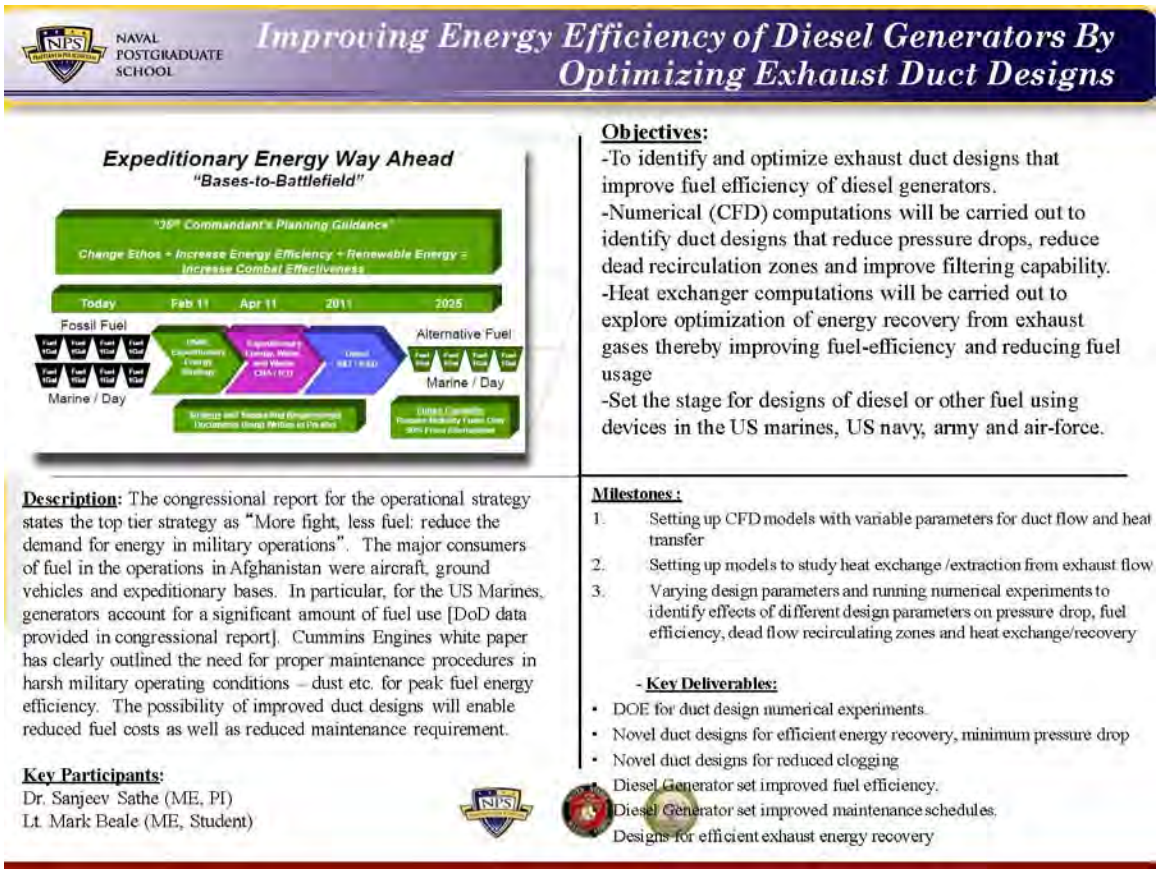

Figure 3. Energy recovery and pressure mitigation proposal from LT Mark Beale and Dr. Sanjeev Sathe to U.S. Marine Corps Expeditionary Energy Office (E2O) (from Sathe & Beale, 2013; Sathe & Millsaps, 2014)

From the acceptance of this proposal, current and future work has been added to the E2O-NPS incentive. While this thesis focuses on the CFD model, additional work is being done on thermal CFD models, infrared (IR) signature reduction, heat exchanger CFD models, design and maintenance of heat exchangers, the supporting infrastructure required for current and additional research, as well as the evaluation of new thermal properties and materials. It is important to note that the exit velocity profiles coming out of the 90^{o} bend studied in this thesis can potentially affect IR signature due to soot loading in the velocity profiles. Also, flow visualization techniques used while studying the effects of turning vane placement offer optimal placement locations for WHR

devices. Figure 4 is the WHRS roadmap outlined by faculty in the Mechanical Engineering Department at NPS.

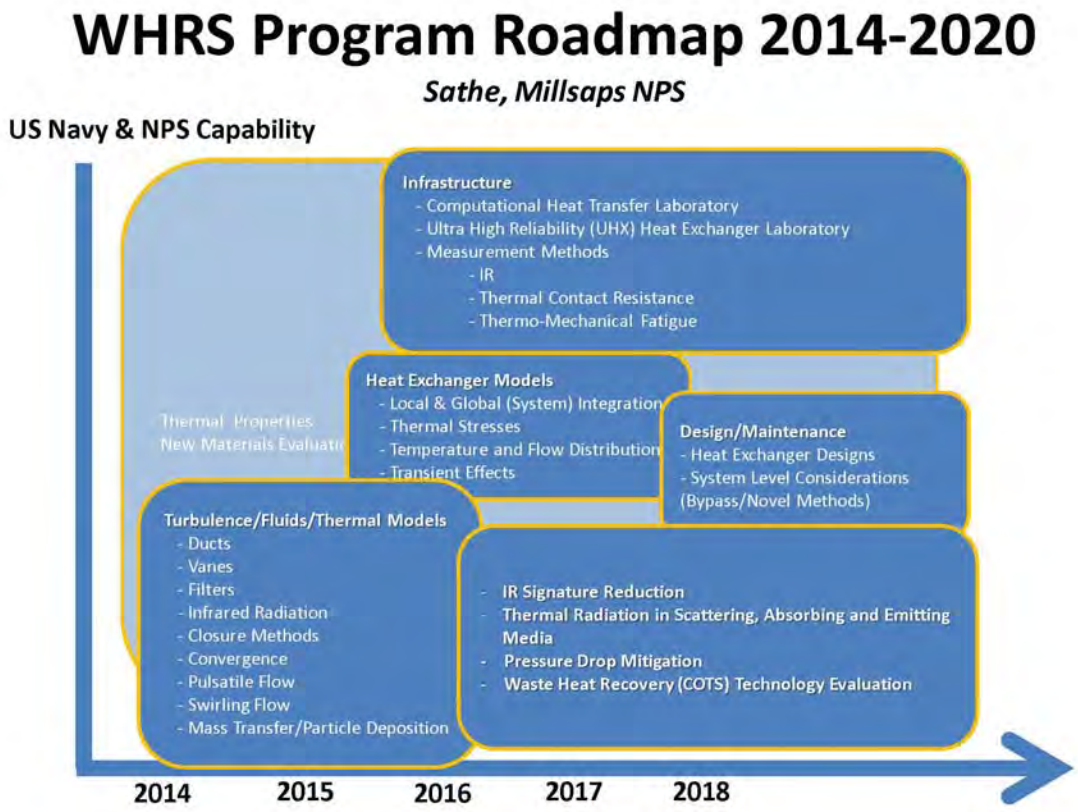

Figure 4. NPS, U.S. Navy and U.S. Marine Corps Waste-Heat Recovery System Roadmap (from Sathe & Millsaps, 2014).

E. OBJECTIVES

The objectives of this thesis were:

- A two-dimensional model that physically represents the real problem.
- Validate the two-dimensional model for both laminar and turbulent flows.
- Vary parameters such as turning vane location, turning vane number and turning vane orientation for optimal results– record and evaluate results related to pressure drop mitigation, recirculation zone size and flow visualization for optimal placement of WHR devices.

II. GOVERNING EQUATIONS AND PARAMETERS

A. CONTINUITY

For the continuity equation used throughout this thesis a two-dimensional approach was taken. The 2D approach simplified the solution and was solved for a "centerline" approximation of a typical three-dimensional circular duct. Cartesian coordinates were used in the 2D case.

$$\frac{\partial \rho}{\partial t} + \vec{\nabla} \bullet \left(\rho \vec{V} \right) = 0 \tag{2}$$

B. NAVIER-STOKES EQUATIONS

As with the continuity equation, the momentum equations were solved for the two-dimensional "centerline" case. The incompressible Navier-Stokes equations are represented in the Cartesian coordinate frame as a result of working in two dimensions. The incompressible momentum equations for Cartesian coordinates are given below, designated by their primary directions (X, Y and Z) for constant density and viscosity.

$$X - dir : \rho \left(\frac{\partial u}{\partial t} + u \frac{\partial u}{\partial x} + v \frac{\partial u}{\partial y} + w \frac{\partial u}{\partial z} \right) = \rho g_x - \frac{\partial p}{\partial x} + \mu \left(\frac{\partial^2 u}{\partial x^2} + \frac{\partial^2 u}{\partial y^2} + \frac{\partial^2 u}{\partial z^2} \right) \tag{3}$$

$$Y - dir : \rho \left(\frac{\partial v}{\partial t} + u \frac{\partial v}{\partial x} + v \frac{\partial v}{\partial y} + w \frac{\partial v}{\partial z} \right) = \rho g_y - \frac{\partial p}{\partial y} + \mu \left(\frac{\partial^2 v}{\partial x^2} + \frac{\partial^2 v}{\partial y^2} + \frac{\partial^2 v}{\partial z^2} \right) \tag{4}$$

$$Z - dir : \rho \left(\frac{\partial w}{\partial t} + u \frac{\partial w}{\partial x} + v \frac{\partial w}{\partial y} + w \frac{\partial w}{\partial z} \right) = \rho g_z - \frac{\partial p}{\partial w} + \mu \left(\frac{\partial^2 w}{\partial x^2} + \frac{\partial^2 w}{\partial y^2} + \frac{\partial^2 w}{\partial z^2} \right) \tag{5}$$

Several assumptions were made for the two-dimensional model, including dropping the Z-terms and neglecting the buoyancy terms in the Navier-Stokes equations. Additionally, time-averaged terms were introduced to model the turbulent flow. These terms, the Reynolds-averaged Navier-Stokes (RANS) terms, are indicated as follows:

$$X-dir:\left[-\frac{\partial\overline{u'u'}}{\partial x}-\frac{\partial\overline{u'v'}}{\partial y}-\frac{\partial\overline{u'w'}}{\partial z}\right] \tag{6}$$

$$Y-dir:\left[-\frac{\partial\overline{v'u'}}{\partial x}-\frac{\partial\overline{v'v'}}{\partial y}-\frac{\partial\overline{v'w'}}{\partial z}\right] \tag{7}$$

$$Z-dir:\left[-\frac{\partial\overline{w'u'}}{\partial x}-\frac{\partial\overline{w'v'}}{\partial y}-\frac{\partial\overline{w'w'}}{\partial z}\right] \tag{8}$$

The RANS equations account for the added shear forces induced by turbulent flow, and these equations are an average value of said shear forces due to the highly variable nature of turbulent flows.

C. DERIVED EQUATIONS FOR MODEL VALIDATION AND NON-DIMENSIONAL PARAMETERS

Non-dimensional parameters are extremely useful due to their wide application across various fluid domains as well as geometric scaling. Reynolds number is used to provide a parameter from which models can be created based on actual flow data for real systems. Comparing non-dimensional pressure drop, velocity and friction factor results against given Reynolds numbers was used to validate both the laminar and turbulent models used in this thesis.

1. Equations for Laminar Model Validation

In order to ensure accuracy with a CFD model and fully understand the nuances of a commercial code, it is necessary to validate all parameters associated with the model and compare to some theoretical or analytical standard. For a two-dimensional flow in which the flow passes between two parallel plates, assuming a no-slip condition at the walls ($\vec{V}$ = 0), we determine that u = u(y) only (thus no X, Z, t dependence). The velocity profile of the fully developed laminar flow between two parallel plates can therefore be shown by the following relationship (White, Fluid Mechanics, 2011):

$$u(y) = -\frac{1}{2\mu}\frac{dp}{dx}\left(D^2 - y^2\right) \tag{9}$$

The variable D is defined as the maximum distance from the centerline of the parallel plates to the plate itself. Figure 5 shows a nominal representation of the development of a laminar flow through two parallel plates with a slug inlet velocity profile (Molki & et al, 2013).

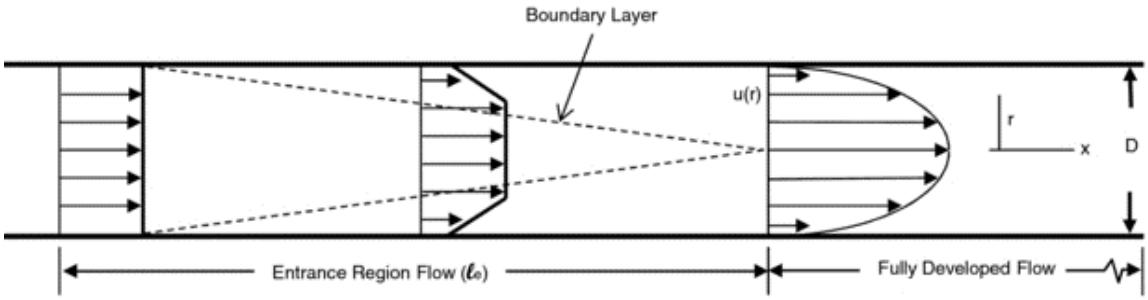

Figure 5. Schematic of flow through two parallel plates, showing laminar fully developed flow (from Anand, 2006).

The entrance length of the duct is a function of Reynolds number and for laminar flow is defined in Equation 14.

$$L_e = 0.06 \cdot \mathrm{Re} \cdot D_h \tag{10}$$

Another form of Reynolds number that was useful for calculations using the two-dimensional model is given by,

$$\mathrm{Re}_h = \frac{\dot{m} D_h}{\mu A} \tag{11}$$

Where $\dot{m}$ is defined as the mass flow rate in [kg/s], D_h is defined as the hydraulic diameter of the duct in [m] given by $D_h = 2D$, μ is the viscosity of the fluid in [kg/m*s] and A is the cross-sectional area of the inlet to the duct. Reynolds number is a measure of the ratio of inertial to viscous forces in any fluid. For the laminar flow regime, Reynolds number is within the range 100<Re<2300. Between 2000<Re<5000 the flow is

characterized as being in the transitional zone between laminar and turbulent flows. Turbulent eddies begin to form as Reynolds number increases. For turbulent flow, Reynolds number is given in the range of $5000<Re<\infty$. For flow where Reynolds number is in the range of $Re>\sim10^6$, Reynolds number dependence in the flow characterization is diminished (White, 2006; Anand, 2006; White, 2011). The results discussion will show that both the USMC field generator and USN LM2500 show characteristics of turbulent flow.

2. Equations for Turbulent Model Validation

Turbulent flow model validation was built from the results gathered in the laminar model validation stage. In order to validate the turbulent model, a comparison against the Darcy friction factor values given on a Moody diagram proved an accurate way to assess whether or not the model would produce accurate results (Idelchik, 1994; Anand, 2006; White, 2006; Kiijarvi, 2011). The Darcy friction factor was calculated using the following relationship:

$$f = \frac{0.316}{\mathrm{Re}^{\frac{1}{4}}} \tag{12}$$

Entrance length for turbulent flows is given by:

$$L_e = 4.4 \cdot D_h \cdot \mathrm{Re}^{\frac{1}{6}} \tag{13}$$

Of particular importance is the realization that for turbulent flows the entrance length to achieve a fully developed profile is significantly less than the entrance length for laminar flows. By comparison, for laminar flow L_e is proportional to Re while in turbulent flow L_e is proportional to $Re^{1/6}$. Throughout this thesis, a slug velocity inlet profile was assumed, thus entrance length calculations were necessary to ensure the inlet portion of the exhaust duct that was modeled in ANSYS/CFX was long enough for the flow to fully develop. For the entrance length calculations to be accurate, the flow had to be fully developed prior to a distance of 3–5 hydraulic diameters from the beginning of the ninety-degree bend.

3. Non-dimensional Parameters

Non-dimensional results are useful in that such results can be applied for a wide range of sizes and velocities. That is to say, a computational model's results are applicable to a real physical system. Pressure drop was calculated in two different ways. The first and more common method is given by:

$$\Delta P^{*} = \frac{\Delta P}{\rho U^{2}}. \tag{14}$$

This non-dimensional parameter is a proportional ratio of pressure differential to pressure head and is useful for noting the effects of kinetic energy on pressure drop.

A second, less-common but very useful means of expressing a non-dimensional pressure drop is given by (Munson, Young, Okiishi, & Huebsch, 2009):

$$\Delta P^{**} = \frac{\Delta P D_{h}}{\mu U}. \tag{15}$$

This term is effectively a ratio of pressure force to viscous force, and draws comparison to Reynolds number.

To study the effects of the recirculation zone caused by the geometry of the 90^{o} duct bend, the following non-dimensional parameter was utilized.

$$b^{*} = \frac{b}{D_{h}} \tag{16}$$

In this relationship, the term b is defined as the average radius of the recirculation zone "bubble." Non-dimensional terms for velocity were given by u^{*}

$$u^{*} = \frac{\bar{u}}{U}, \tag{17}$$

where $\bar{u}$ is defined as the average velocity at a given location along the duct and U is defined as the inlet velocity.

Other interesting non-dimensional parameters associated with the turning vane include non-dimensional chord length, where chord length is defined as the length from tip-to-tail of an airfoil:

$$c^* = \frac{c}{D_h} \tag{18}$$

Additionally, non-dimensional radius, r^* and non-dimensional thickness, t^* are defined below:

$$r^* = \frac{r}{D_h} \tag{19}$$

$$t^* = \frac{t_{\max}}{c} \tag{20}$$

For the non-dimensional radius, r is the nominal radius of curvature of the turning vane and D_h is the hydraulic diameter. For the non-dimensional thickness, t_{max} is the maximum thickness of the turning vane and c is the chord length.

For scaling purposes, it is necessary to non-dimensionalize parameters such as length and diameter in order to provide a wide range of applicability of results from model runs. For this reason, D^* is defined as:

$$D^* = \frac{D_h}{L} \tag{21}$$

Other geometric parameters are given below:

$$x^* = \frac{x}{L} \tag{22}$$

Here, x represents distance in [m] from the origin along the horizontal and L is the overall length of the inlet portion of the exhaust duct in [m].

$$y^* = \frac{y}{H} \tag{23}$$

Here, y represents the distance in [m] from the origin along the vertical and H is the overall height of the outlet portion of the exhaust duct.

4. Non-dimensional Parameter Ranges for Navy and Marine Corps Systems

Table 1 illustrates the range of non-dimensional values expected for the U.S. Navy's LM2500 main propulsion engine as well as the U.S. Marine Corps' MEP-803A field generator set. This information is taken from the data sheets for both the MEP-803A and the LM2500.

	USMC/GENSET	USN/LM2500
D* ranges	0.4	0.6
Re ranges	13,000 – 18,000	500,000 – 2,000,000

Table 1. Range of non-dimensional parameter values for the Navy and Marine Corps systems.

THIS PAGE INTENTIONALLY LEFT BLANK

III. NON-DIMENSIONAL MODEL GEOMETRY

The purpose of using non-dimensional geometric factors throughout this thesis study is to allow a wide application of the gathered results over a broad spectrum of applications. Since much of this study is for application in WHR devices in various Navy and Marine Corps systems, it was prudent to use non-dimensional features in order to evaluate different systems simultaneously and with minimal computing time. The non-dimensional parameters discussed in Chapter II are illustrated in Figure 6.

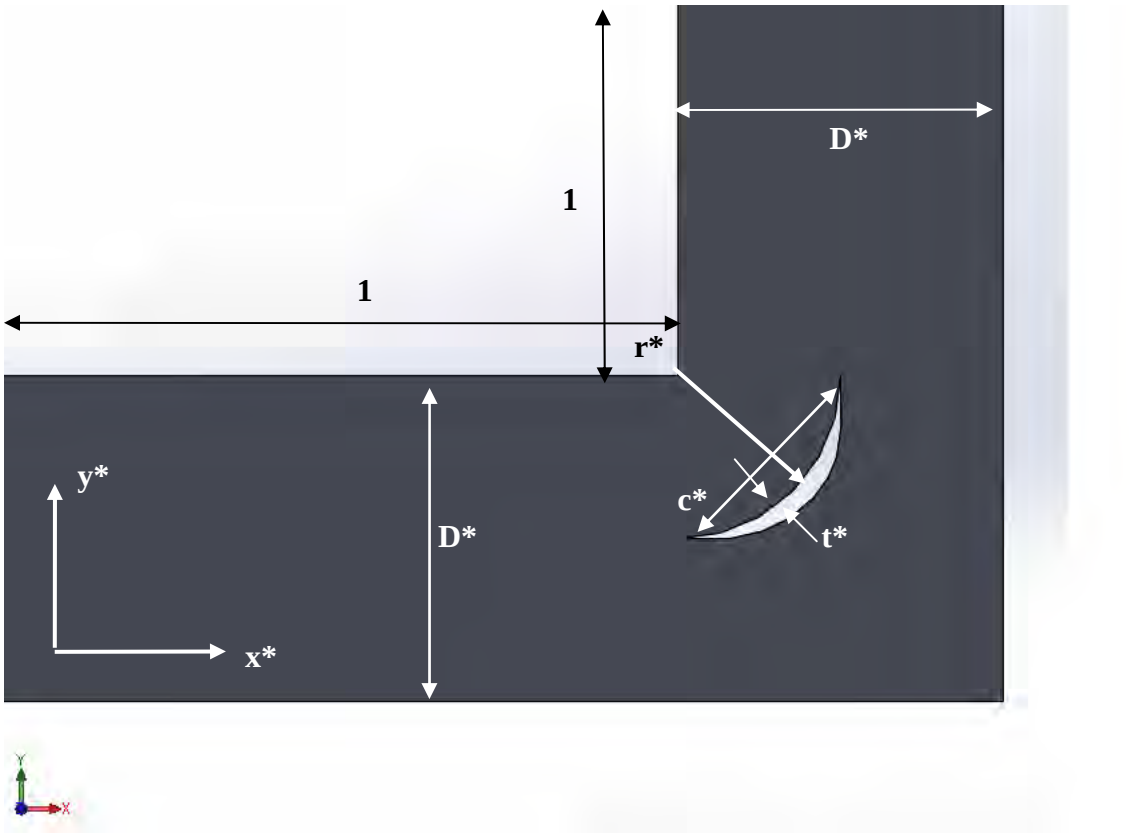

Figure 6. Non-dimensional geometry of 90^{o} exhaust duct with one turning vane in XY plane.

The exhaust ducts utilized by the Navy and Marine Corps systems are typically circular in shape, thus a cylindrical approach to the continuity and momentum equations

would have been appropriate for such a case. However, as mentioned in previous sections, the purpose of using a two-dimensional Cartesian approach was to simplify the real-world three-dimensional problem. The two-dimensional Cartesian approach greatly simplified computational time as well as simplified convergence of the model results. Attaining convergence in ANSYS/CFX was necessary to ensure accuracy of results, which in turn was necessary to validate the model used.

The non-dimensional parameters shown in Figure 6, and defined in Chapter II-C-4, were useful in comparing results for the various runs conducted for model validation, as well as for the collection of results. Because of the use of non-dimensional geometric parameters varying geometry did not infer starting the problem over from scratch. Rather, by varying specific parameters one at a time optimal results were attained by building upon the results of previous runs.

IV. LAMINAR MODEL VALIDATION

A. MESH SIZING

Proper mesh sizing was critically important in ensuring model convergence. Having too coarse of a mesh resulted in divergent solutions, while too fine of a mesh oftentimes did not yield any more accurate of a solution than a mesh that was not extremely fine. The computing time required for an extremely fine mesh was excessive. In addition, for extremely fine meshes it was found that the solution did not properly average the eddy formation phenomenon, which is observed using an appropriately sized mesh. The turbulence models used in this thesis rely on a false time step and use an average value function; the smaller the time step and the more fine the mesh the more closely the problem resembled a real-world situation, for which there is not an applicable model. However, for the laminar model used in this thesis turbulence was neglected and solutions were deemed accurate on whether or not they satisfied a fully developed profile.

In order to determine the proper geometry from which to run the laminar (and eventually the turbulent) models, measured data from the Marine Corps' MEP-803A field generator was used. This data included temperature and mass flow rate measured in the exhaust. Scaling this flow for a model that would run efficiently and effectively, Reynolds number relationships were used to scale the model. Appendix A contains the details of the geometry set-up used in SolidWorks and ANSYS. Appendix B contains ANSYS/CFX set up for mesh sizing and CFX-PRE input parameters for laminar and turbulent runs.

B. EVALUATION OF VALIDATION RESULTS

Velocity profile data was extracted from the laminar model by selecting data along the inlet portion of the exhaust duct. This velocity profile was compared to nominal values calculated using the input criteria for the run. A nominal value for the maximum

velocity of the fully developed laminar profile was determined to be 0.586 [m/s]. Figure 7 shows a plot of velocity data at specific locations along the x-direction.

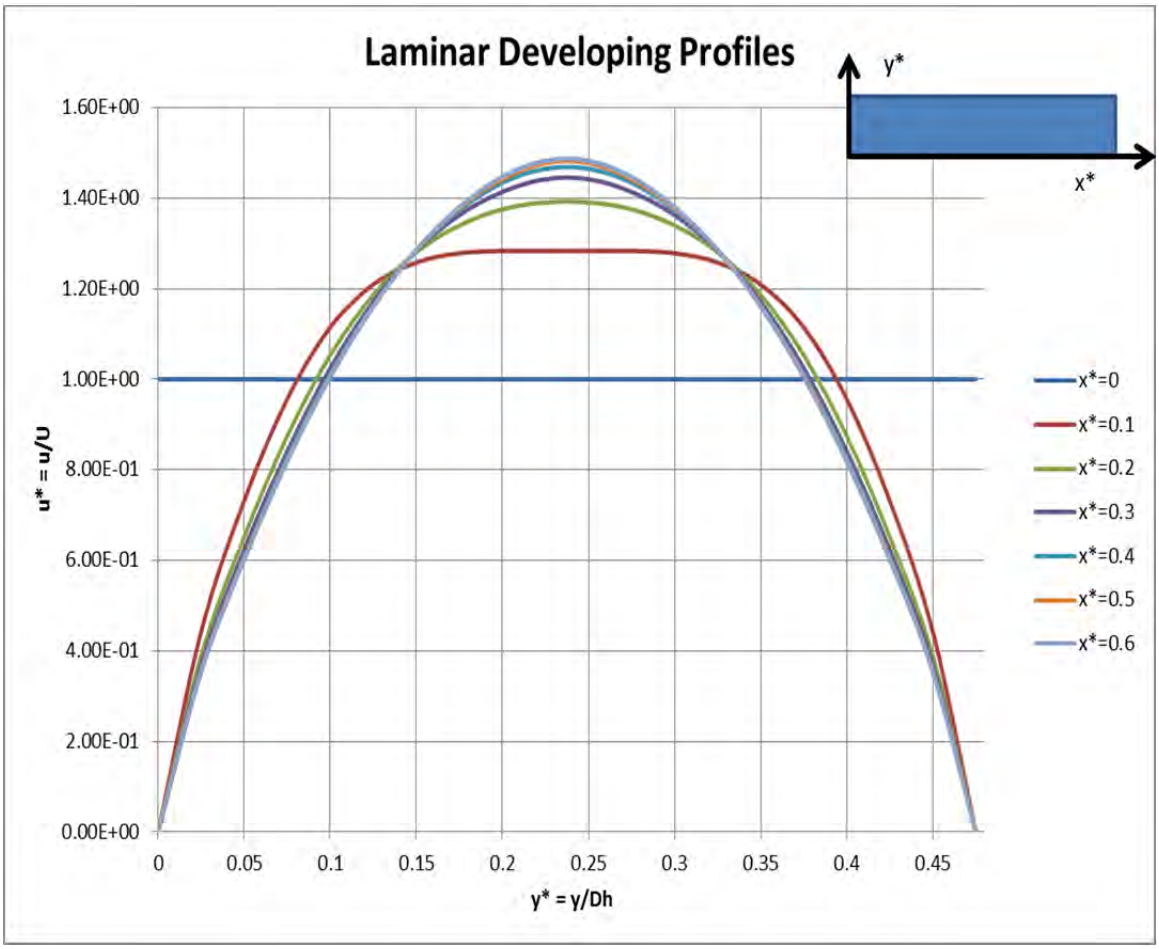

Figure 7. Velocity developing profiles for laminar model validation runs.

What the plot in Figure 7 shows is the development of the flow from a slug inlet profile (where velocity is uniform across the cross-section of the duct inlet) to a fully developed laminar profile. The maximum value for the flow velocity at the calculated entrance length of $x^* = 0.6$ was determined to be $u^* = 1.5$. The values collected from the laminar model runs match the expected theoretical values, thus resulting in a positive step in laminar model validation.

The dynamic viscosity of the working fluid (air) was modified as an additional step in model validation. In doing so, the expected values for the maximum flow velocity for the fully developed laminar profile also increased and decreased by a factor of ten, respectively. By adjusting mass flow rate for the newer viscosities, Reynolds number was maintained at a value of 1000 for laminar flow. The velocity profiles for each run were compared to known theoretical values based on the input velocity for each flow condition and validated against said known values. From these runs the model was determined to be valid. By validating the model in the laminar flow regime, a base of results could be used to further validate the model in the turbulent flow regime.

THIS PAGE INTENTIONALLY LEFT BLANK

V. TURBULENT MODEL VALIDATION

A. MESH SIZING

As a result of validating the laminar model, the geometry and mesh used were applied to the turbulence model. Appendix A references the values used for geometric and mesh set up for turbulence validation. Appendix B contains the input parameters for ANSYS/CFX-PRE used.

B. ANSYS/CFX SET-UP

The turbulent validation depended highly on varying Reynolds number and comparing friction factor results against a Moody Diagram. In order to achieve accurate results, the setup in CFX-PRE was critical. Appendix B contains the set-up inputs for the model runs. An important discussion arose when determining which turbulent model to use. The k-ε model is widely accepted as an accurate method of applying RANS equations to a turbulent model (Patankar, 1980). In this thesis, the k-ε model was used as the turbulence model, while turbulence intensity values were used to determine the intensity of the actual flow being simulated. The k and ε values were determined from the input turbulence intensity level prior to commencing simulation runs.

C. EVALUATION OF VALIDATION RESULTS

To validate the turbulent model several runs were conducted at various Reynolds numbers to determine the Darcy friction factor for each run. These values were taken from the straight inlet portion of the exhaust duct and are tabulated in Table 2. Graphical results are plotted on a Moody diagram in Figure 8.

	Darcy Friction Factor, Smooth	
Reynolds Number [1]	CFD Results	Theoretical Values
4900	0.0378	0.0380
6000	0.0360	0.0360
7000	0.0345	0.0340
8100	0.0333	0.0330
9200	0.0323	0.0320
25600	0.0250	0.0260
76800	0.0190	0.0200
12800	0.0167	0.0170

Table 2. CFD Darcy friction factor calculations at varying Reynolds numbers.

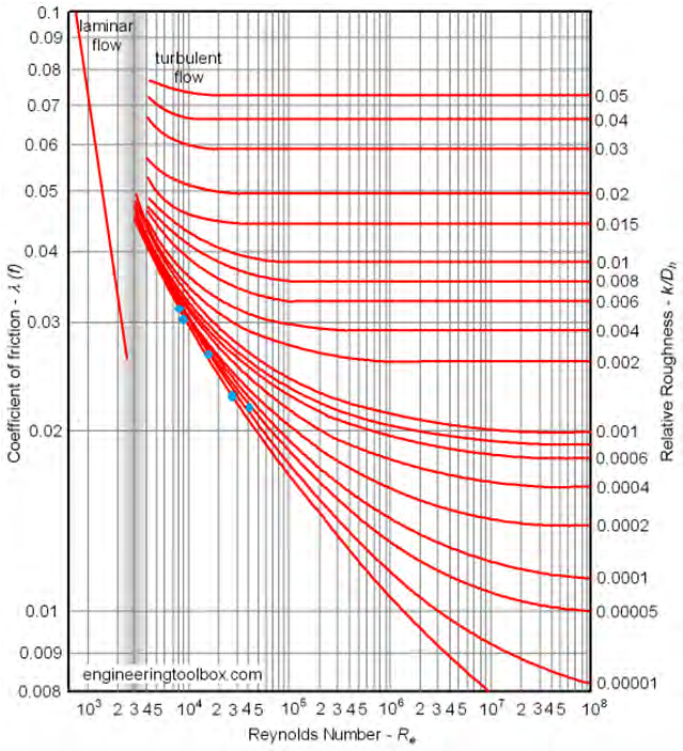

Figure 8. Moody diagram showing plotted Darcy friction factor value lines, with point value data for CFD results (from Kiijarvi, 2001)

The Moody diagram in Figure 8 is a plot showing the effect of increasing the Darcy friction factor, f over a range of Reynolds numbers. For a smooth pipe, where relative roughness is 0, the Blausius equation can be used to approximate the value of the friction factor, which shows that $f \propto \mathrm{Re}^{-1/4}$. The exact equation used is shown by Equation (12). The results plotted show that as Reynolds number increases, the friction factor decreases. This result can be explained by the definition of Reynolds number. Reynolds number physically represents the ratio of inertial forces to viscous forces. By increasing the velocity of the flow, represented in the inertial forces, the ratio of the inertial to viscous forces increases.

THIS PAGE INTENTIONALLY LEFT BLANK

VI. DISCUSSION OF RESULTS

A. VELOCITY PLOT FOR NO TURNING VANE CASE

Figure 9, shown below, represents the baseline model used in this thesis. There are no turning vanes located in the ninety-degree bend, and a discussion of these results follows. The velocity scale used shows values of v^*.

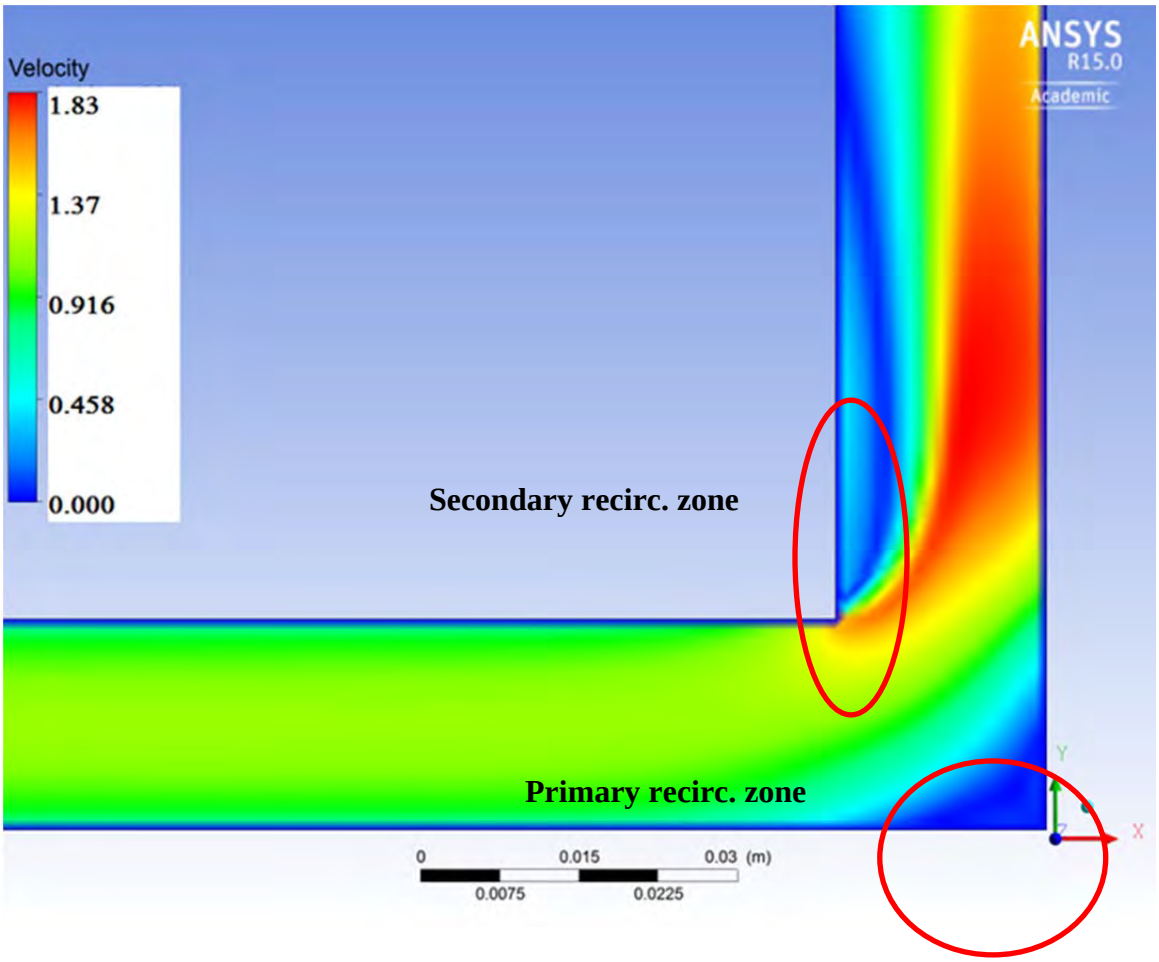

Figure 9. Non-dimensional velocity profile of 90^o bend without a turning vane for Re = 76,800, D^* = 0.04.

In Figure 9, the non-dimensional velocity plot provides a great deal of insight with regard to backpressure reduction, WHR device placement as well as recirculation zone size, which is related to soot deposition and accumulation. Proceeding along the

inlet portion from left to right, a uniform, fully developed turbulent profile is shown. Once the flow encountered the 90^o bend, it appeared as if the flow became constricted, as if the hydraulic diameter was artificially reduced due to the geometry presented by the bend. This is the case, as noted in by Idelchik (Idelchik, 1994). As mentioned in Chapter I, the flow experienced a drastic shift in momentum in the bend due to changing of flow direction, and viscous forces increased in this region as a result of said momentum shift. As the flow proceeded out of the bend and along the outlet portion of the exhaust duct a non-uniform velocity profile characterized the flow. Recirculation zones appeared in the bottom-right corner of the bend as well as in the left side of the initial portion of the outlet of the exhaust duct.

A few key takeaways from Figure 9 will be used throughout the remainder of the discussion. First, the primary recirculation zone located in the bottom right portion of the 90^o bend may cause flow blockage and could also be a possible site for soot and particle deposition, which will further add to blockage and increase time and money spent in maintenance of the exhaust duct. Shown in Chapter VI-B is the effect of the application of a turning vane placed in the 90^o bend for the same inlet and outlet boundary conditions that were applied to give the results in Figure 9; the primary recirculation zone does diminish in size but does not completely disappear. Second, the optimal placement of a WHR device, from initial observation and flow visualization, is to place the device in a location further away from the bend so as to experience more uniform flow distribution. Exit velocity profiles are shown in Chapter VI-C and show that the flow developed from a non-uniform exit velocity profile to a more uniform profile. Third, the secondary recirculation zone located in the left side of the initial portion of the outlet of the exhaust duct will drive the shape of the exit velocity profile and could be the epicenter for unwanted vibrations due to large pressure and velocity differentials confined to a localized region in the outlet.

B. VELOCITY PLOT FOR ONE TURNING VANE CASE

Figure 10 shows the results for a single large vane placed centrally in the exhaust duct ninety-degree bend. A discussion of these results follows. The velocity scale used shows values of v^*.

In Figure 10, a turning vane is introduced in the 90^o bend. When compared to Figure 9, some immediate differences are noted. First, both the primary and secondary recirculation zones have diminished in size, and their effect on the flow is reduced. Second, improved flow velocity distribution occurs more rapidly in the one vane case compared to that of the no vane case; that is to say, the flow becomes more uniform more rapidly in the case of one turning vane compared to that of the no vane case. The reason for the occurrence of both primary and secondary recirculation zones can best be described as an effect of boundary layer separation caused by a drastic change in the wall geometry (Idelchik, 1994; Schlichting, 1979).

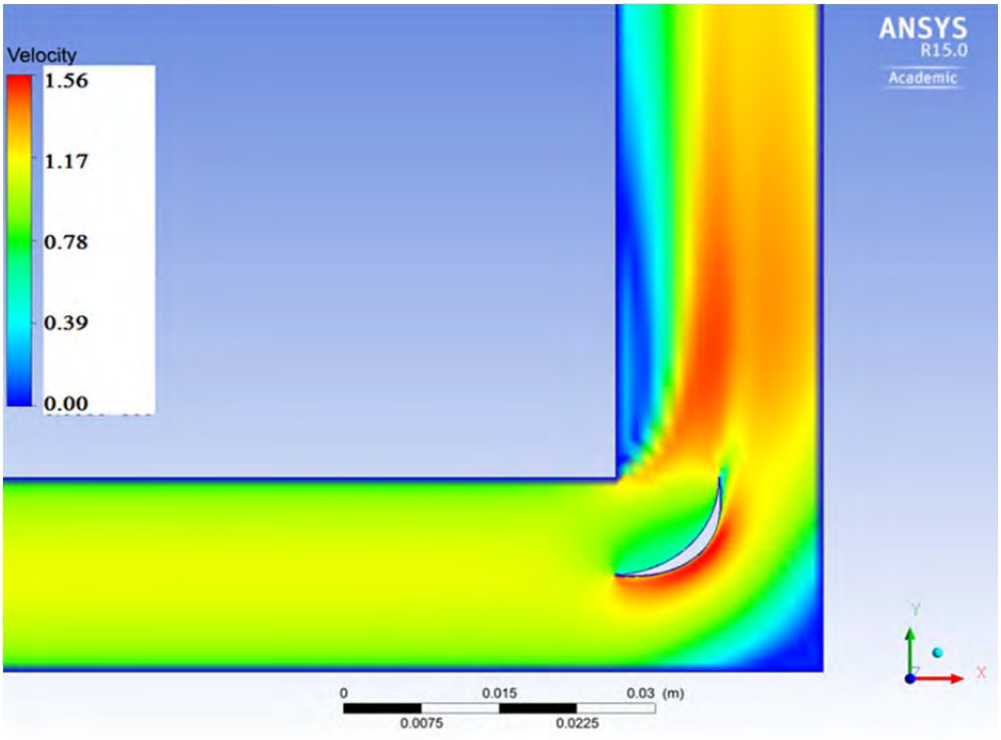

Figure 10. Non-dimensional velocity profile of 90^o bend with one turning vane for Re = 76,800, $D^* = 0.04$, $c^* = 0.35$, $r^* = 0.4$, $t^* = 0.07$.

Significant improvement in the flow is shown by the addition to a simply shaped turning vane as shown in Figure 10. Despite drastic improvements compared to the results plotted in Figure 9, additional improvements in the flow were characterized by shifting the location of the turning vane toward the upper left corner of the bend, thus reducing the secondary recirculation zone significantly and showing even greater pressure drop values. Chapter VI-D shows the effect of a turning vane placed in the upper left corner of the 90^{o} bend.

C. EXIT VELOCITY PROFILE FOR OUTLET PORTION OF EXHAUST DUCT

Figures 11–12 show the results of the velocity vectors for a single large vane placed centrally in the exhaust duct ninety-degree bend. A comparison of the velocity vectors located nearest the ninety-degree bend to the velocity vectors further from the ninety-degree bend is noted in the discussion, which follows. The velocity scale used shows values of v^{*}.

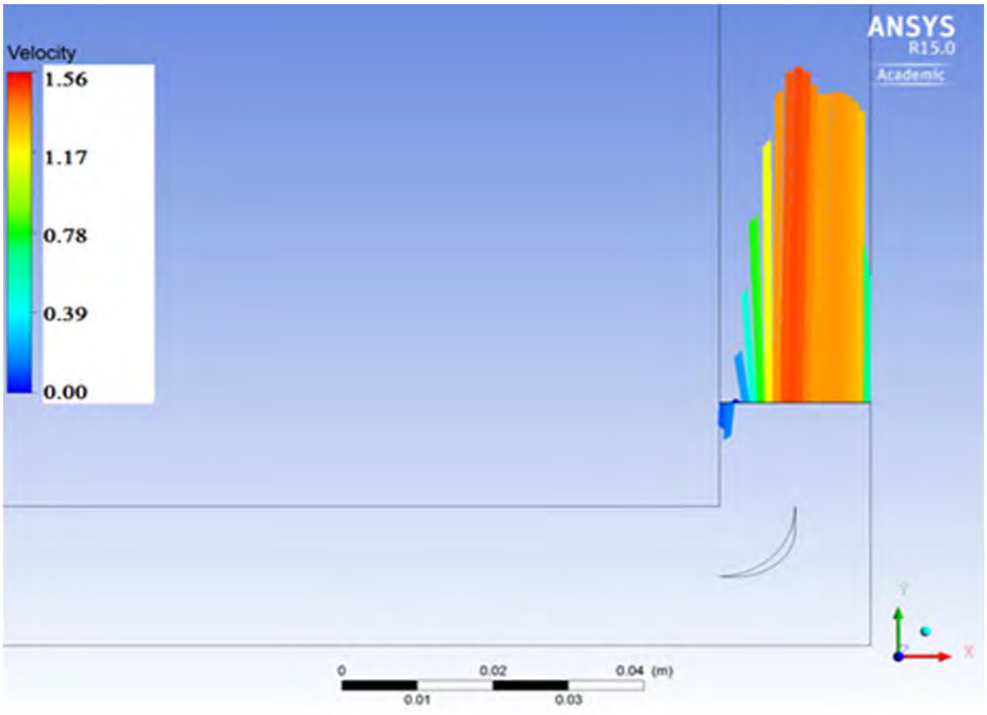

Figure 11. Non-dimensional exit velocity profile for 90^{o} bend, showing effect on velocity profile near the bend for Re = 76,800, D^{*} = 0.04, c^{*} = 0.35, r^{*} = 0.4, t^{*} = 0.07.

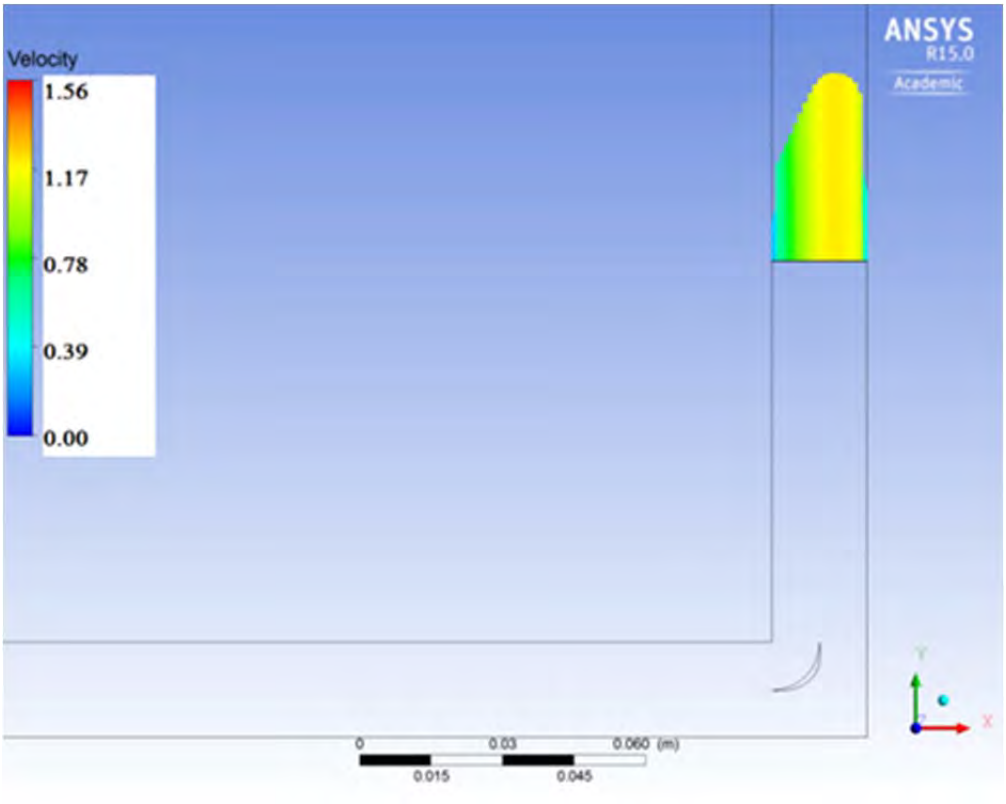

Figure 12. Non-dimensional exit velocity profile for 90^{o} bend, showing effect on velocity profile far downstream for Re = 76,800, D^{*} = 0.04, c^{*} = 0.35, r^{*} = 0.4, t^{*} = 0.07.

Figures 11 and 12 are plotted non-dimensional exit velocity profiles at two separate locations with respect to the 90^{o} bend. Figure 11 shows the effect on the velocity profile nearest the bend, while Figure 12 shows the effect on the velocity profile further away from the bend. The non-uniform profile as discussed in Chapter VI-B is clearly evident in Figure 11. The portion of the profile closest to the left side of the duct outlet demonstrated a negative velocity gradient, indicating counter-flow in this region. This counter-flow explains the effect of the secondary recirculation zone on the flow and also provides and insight into the source of possible backpressure in this region. Figure 12 is indicative of a more uniformly distributed velocity profile further downstream, though the effects of the 90^{o} bend geometry are still evident in its shape. Results from Figure 12 in particular provided a great insight into optimal WHR device placement, and also may

provide insight into future work with IR signature reduction and possible soot loading of the exhaust gases shown as a probability density function with respect to u^* and D_h.

D. VELOCITY PLOT FOR A TURNING VANE PLACED IN THE UPPER LEFT CORNER OF 90^O DUCT

Figure 13, illustrated below, shows the results for a single small vane placed optimally in the upper left corner of the exhaust duct ninety-degree bend. A discussion of these results follows. The velocity scale used shows values of v^*.

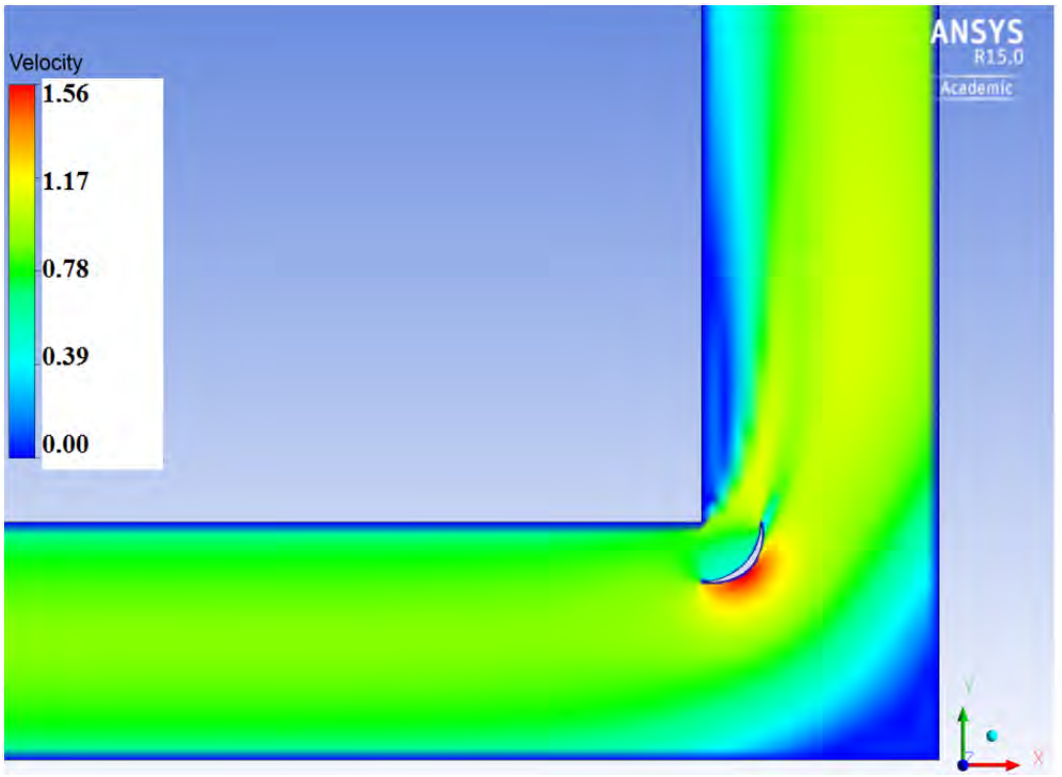

Figure 13. Non-dimensional velocity profile of 90^o bend with one turning vane located near the upper left corner for Re = 76,800, D^* = 0.04, c^* = 0.18, r^* = 0.2, t^* = 0.07.

The results from Figure 13 illustrated the epitome of the study conducted in this thesis. By optimally placing the turning vane in the upper left corner of the 90^o bend, noticeable difference in the velocity profile is seen between this result and the results

shown in Figure 10. Some remarkable observations were made with regard to Figure 13. First, the magnitude of the velocity is nearly constant throughout the bend, resulting in a significantly diminished secondary recirculation zone as well as a slight reduction in the primary recirculation zone as compared to the case of no vane in Figure 9. Second, the velocity exit profiles are more uniform in the outlet portion of the duct, thus allowing for more leeway in WHR device placement. Third, and as discussed in Chapter VI-H, reduction in pressure drop is on average 10% better than the case of a single turning vane placed centrally in the 90^o bend.

The CFD results shown in Figure 13 are extremely important moving forward in the energy recovery and energy harvesting programs. Not only is contemplation of a turning vane a factor in design considerations, but a decision on vane placement is now a critical factor in the design process for optimal location of WHR devices, as well as for significant reduction in backpressure leading to improved fuel economy and decreased money spent on fuel.

E. PRESSURE CONTOUR FOR NO TURNING VANE CASE

The results from Figure 14, below, show the nominal pressure drop that occurs due to the 90^o geometry without the effect of a turning vane. The recirculation zones played a vital role in determining the value of the pressure drop across the duct. Of note, all sources consulted for estimated head loss over a simple 90^o bend assumed that the inlet profile was a slug inlet velocity profile, thus estimating head loss coefficients under this assumption. Since the velocity profile entering the inlet portion of the 90^o bend in this case was determined to be a fully developed turbulent profile, head loss values and coefficients were determined to be proportionally greater than expected head losses. When head loss was calculated over the entire domain for the 90^o bend (that is to say, from $x^* = 0$ to $y^* = 1$) the calculated values were within 12% of the values of the head loss coefficient, K_L, reported in Idelchik's *Handbook of Hydraulic Resistance* (Idelchik, 1994) for sharp bends.

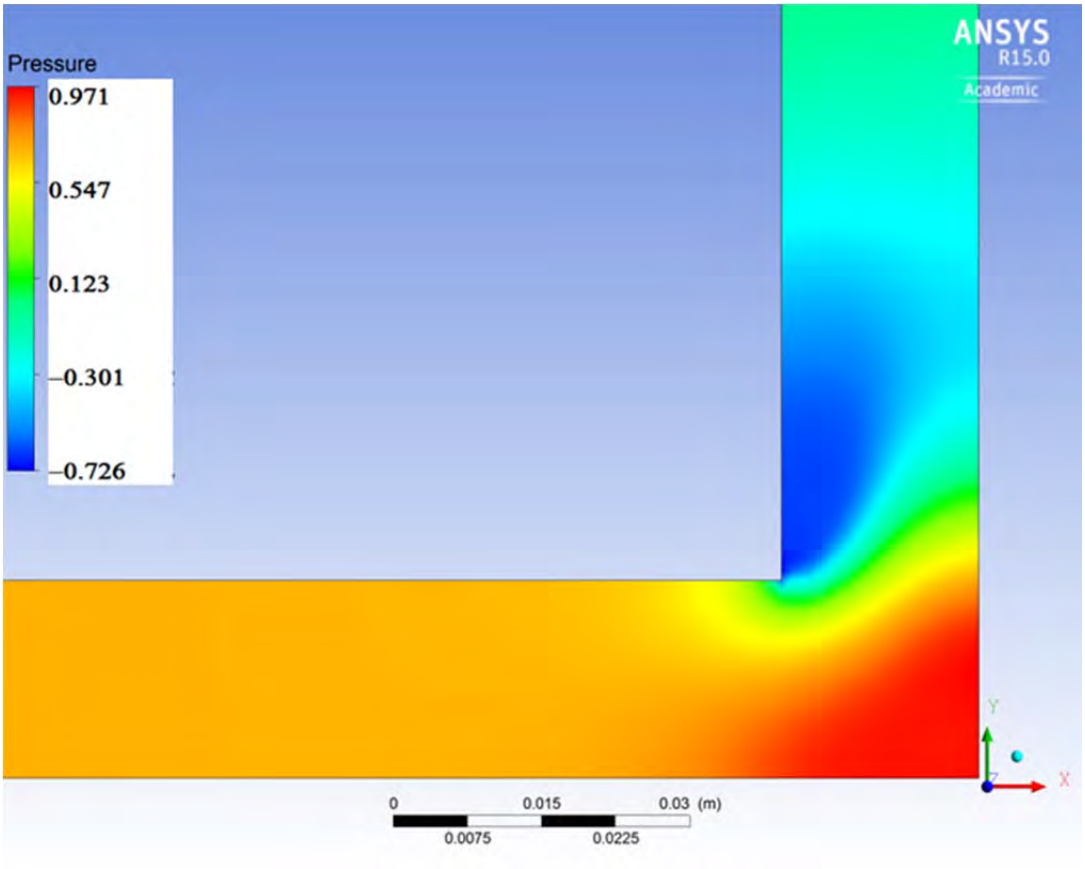

Figure 14. Non-dimensional pressure profile for 90^{o} bend without a turning vane for Re = 76,800, D^{*} = 0.04.

F. PRESSURE CONTOUR FOR ONE TURNING VANE CASE

The effect of one turning vane demonstrated in Figure 15, below, on the pressure drop across the bend is drastic in comparison with Figure 14. Both the primary and secondary recirculation zone pressure effects have been minimized and the overall drop in pressure across the bend is on average 50–60% less with one turning vane that without a turning vane. The significance of this is that backpressure will be greatly reduced in the exhaust duct, allowing for greater fuel economy and a less-restricted flow available to WHR devices.

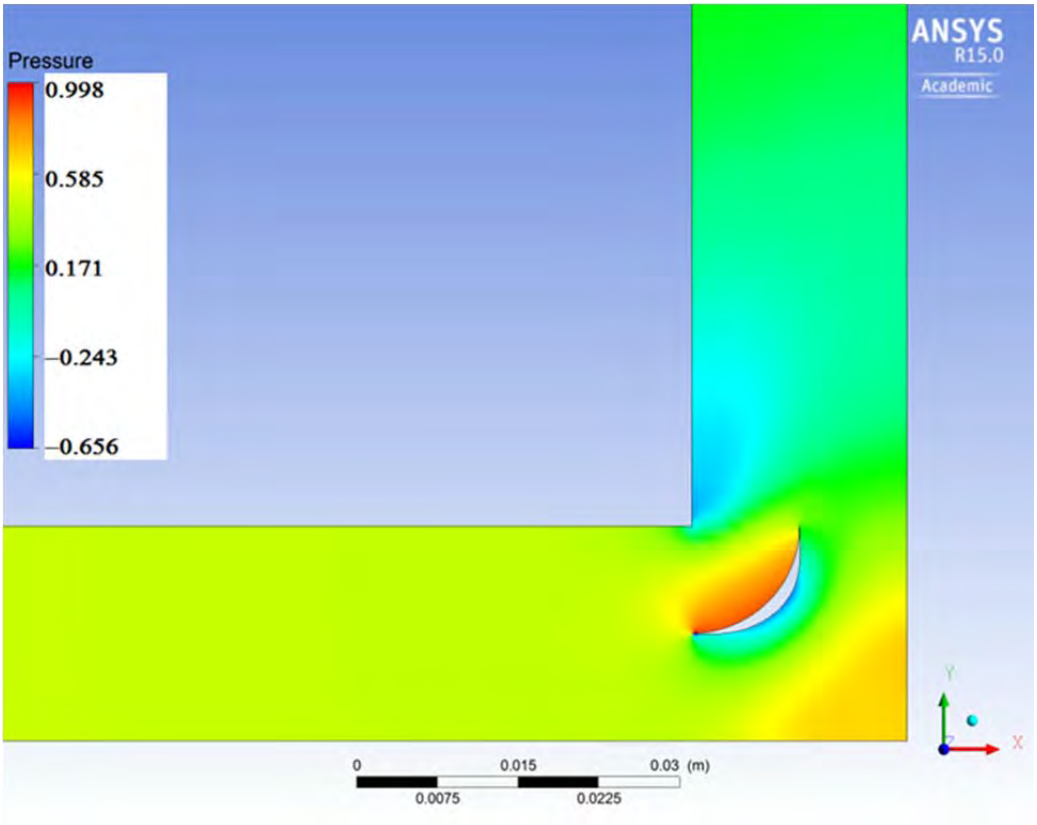

Figure 15. Non-dimensional pressure profile for 90^{o} bend with a turning vane for Re = 76,800, D^{*} = 0.04, c^{*} = 0.35, r^{*} = 0.4, t^{*} = 0.07.

G. PRESSURE CONTOUR FOR ONE TURNING VANE PLACED IN THE UPPER LEFT CORNER OF A 90^{O} DUCT

In comparison with Figure 15, the results from Figure 16 illustrated below appear to show an increased pressure drop by placing the turning vane in the upper left corner of the exhaust duct bend. However, as shown in Chapter VI-H in the plotted data for the pressure drop comparison, the reduction in pressure drop in the case of Figure 16 is actually 10% greater than that of the case of Figure 15. What these results show is that the primary impact on backpressure is attributed to the magnitude of the secondary recirculation zone rather than the primary recirculation zone. This conclusion is appears to be counter-intuitive, however upon further investigation this conclusion is sound for a few reasons.

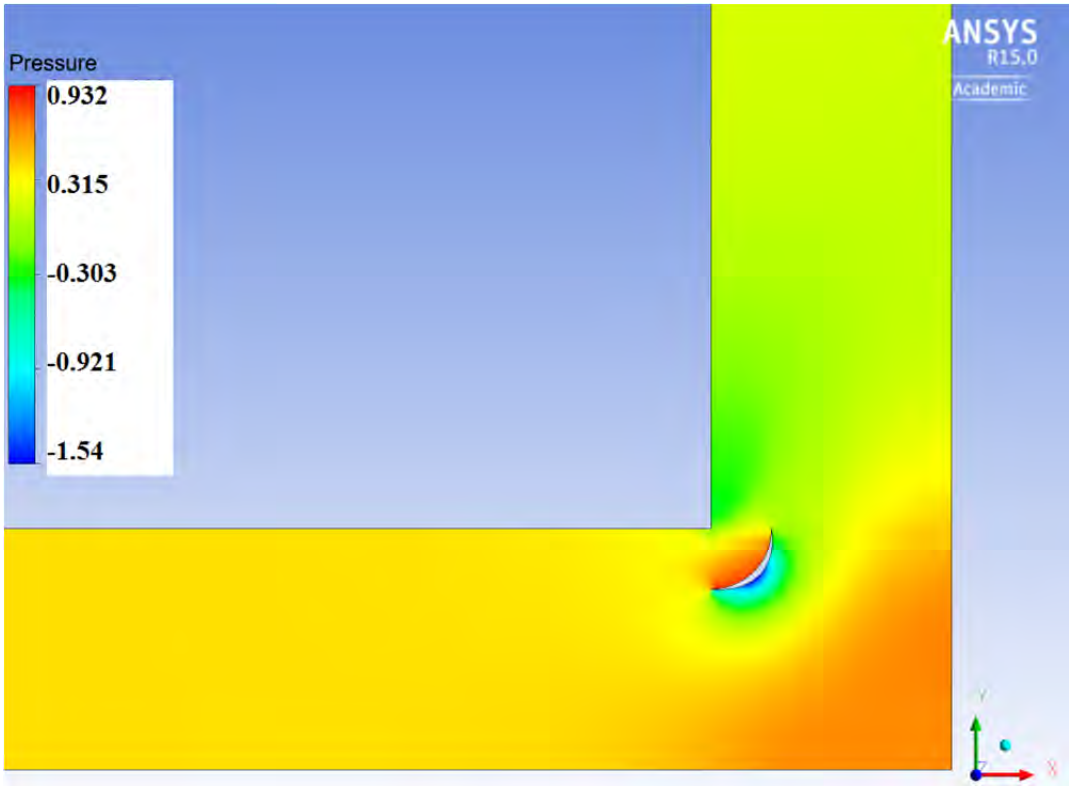

Figure 16. Non-dimensional pressure profile for 90^{o} bend with a turning vane placed in upper left corner of duct bend for Re = 76,800, D^{*} = 0.04, c^{*} = 0.18, r^{*} = 0.2, t^{*} = 0.07.

First, the variation in size of the primary recirculation zone does not immediately show any correlation to increase in backpressure. Rather, the primary recirculation zone can be thought of as a “dead zone” where flow velocity approaches zero and at no time has an overall negative gradient against the primary direction of the flow. Second, the secondary recirculation zone does show a negative gradient against the primary direction of the flow as indicated in the exit velocity profiles shown in Figure 11. Third, the effect of the secondary recirculation zone on constricting the flow by reducing the effective hydraulic diameter proportionally more than the primary recirculation zone leads to the conclusion that backpressure can most consistently be attributed to the secondary recirculation zone size for the 90^{o} sharp-cornered bend. Since the effective hydraulic diameter along the diagonal from the upper left to bottom right of the bend is greater than the actual hydraulic diameter of the duct itself, the size of the primary recirculation zone

did not fully impede the flow from passing through the inlet portion of the bend. Once the flow encountered the outlet portion of the bend, boundary layer separation that occurred at the upper left corner of the bend resulted in the creation of the secondary recirculation zone and thus restricted the passage of the flow through this portion of the outlet of the exhaust duct.

H. EFFECT OF VARIOUS VANE CONFIGURATIONS ON PRESSURE DROP IN A 90^{O} EXHAUST DUCT BEND

Several vane configurations were evaluated through the course of this thesis. Vane orientation, size and location were altered to study the effects of the pressure drop across the sharp 90^{o} turning bend. In order to optimize pressure drop through the bend the results of changing the vane configuration were plotted against each other in order to evaluate the results and draw conclusions on which vane configuration would be best suited for energy efficiency.

The pressure drop was calculated as an average across the sharp-cornered 90^{o} duct bend at a distance of one non-dimensional hydraulic diameter from the beginning and end of the sharp bend. Figure 18 shows this pictorially. The results from the averaged pressure drop across the 90^{o} bend were plotted in Figure 17, shown below in subsection 1. Figures 19–22 show the different vane configurations that were studied in this thesis, ranging from a centered vane to a three-vane configuration.

For simplification of evaluating the results, the results for P^{*} and P^{**} are organized into Chapter VI-H-1 for P^{*} and Chapter VI-H-2 for P^{**}. As a consequence of plotting pressure drop using two different calculation methods, different conclusions can be drawn as explained in each subsection. Additionally, the effect of the various turning vane configurations on the recirculation zone size is explained in Chapter VI-H-3. Figures 24, 25 and Table 5 aid in this discussion.

1. Plotted Results for ΔP^*

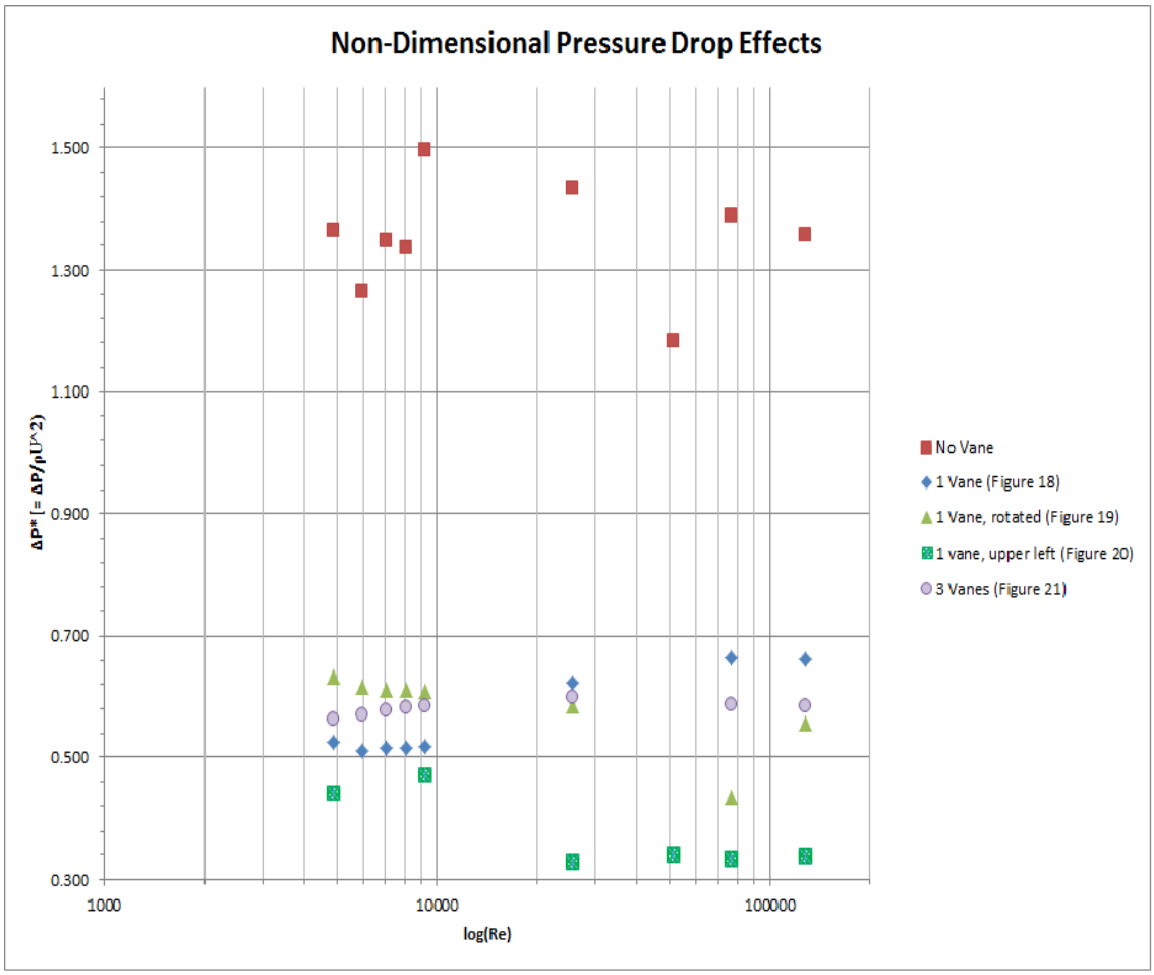

Figure 17. Non-dimensional pressure drop values for ΔP^* in an exhaust duct with a 90^o bend.

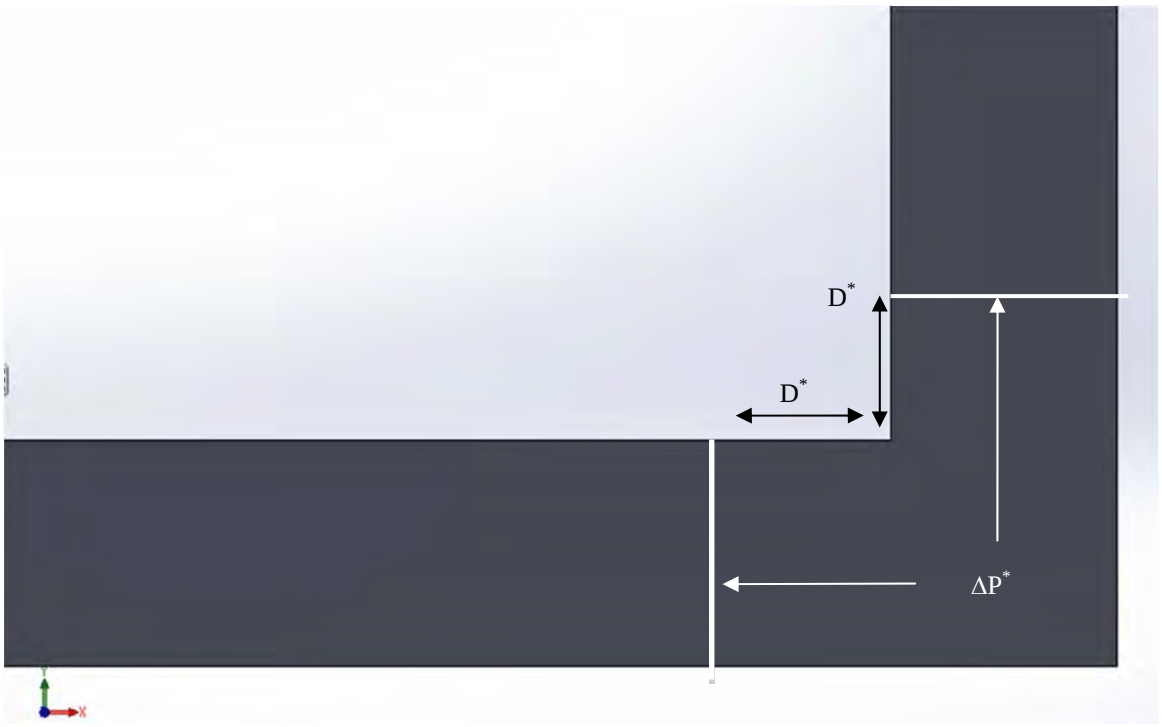

Figure 18. Non-dimensional locations of pressure drop calculations for 90^{o} bend.

The effect of placing a single vane in a 90^{o} bend is illustrated in Figure 17. Figure 18 shows the non-dimensional location from which ΔP^{*} and ΔP^{**} were calculated. Several vane configurations were considered when comparing to the no vane case, to include a turning vane translated into the upper left corner of the bend, a turning vane that was rotated counter-clockwise, a three-vane configuration, and a single vane placed centrally in the bend. Figures 19–22 show these vane configurations:

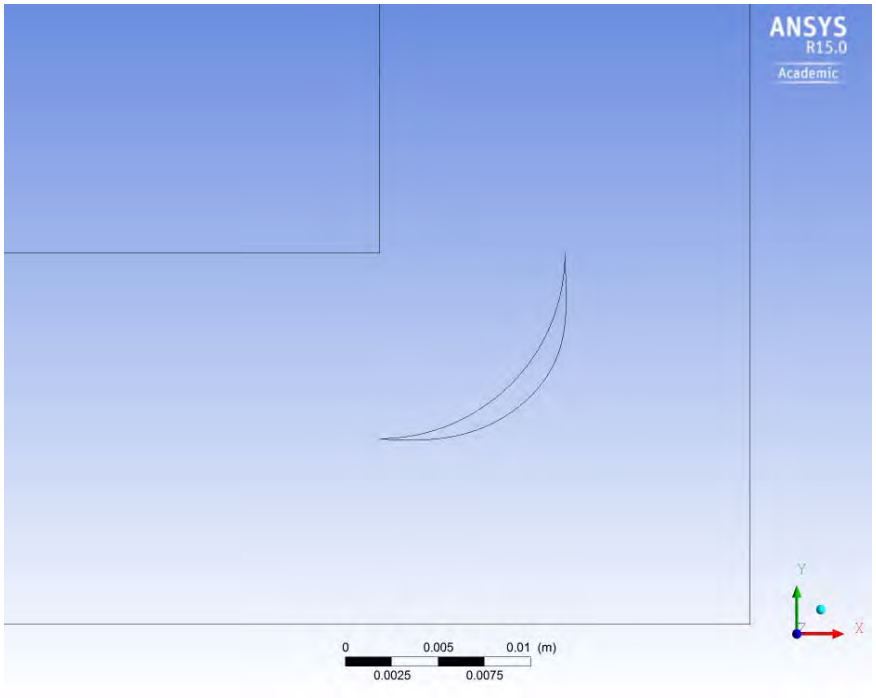

Figure 19. Profile view of one vane configuration for $D^* = 0.04$, $c^* = 0.35$, $r^* = 0.4$, $t^* = 0.07$.

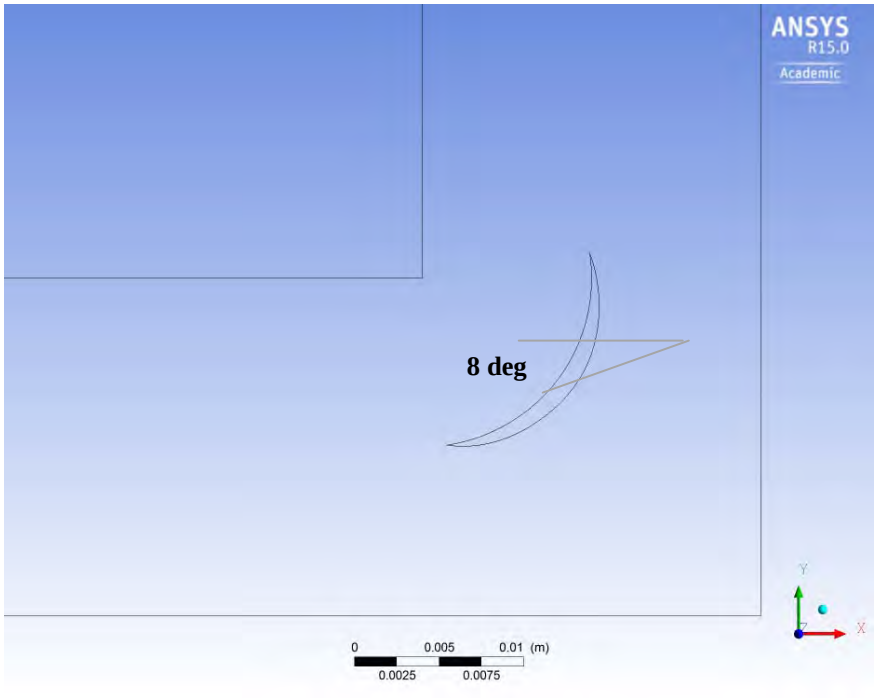

Figure 20. Profile view of one vane rotated counter-clockwise from horizontal configuration for $D^* = 0.04$, $c^* = 0.35$, $r^* = 0.4$, $t^* = 0.07$.

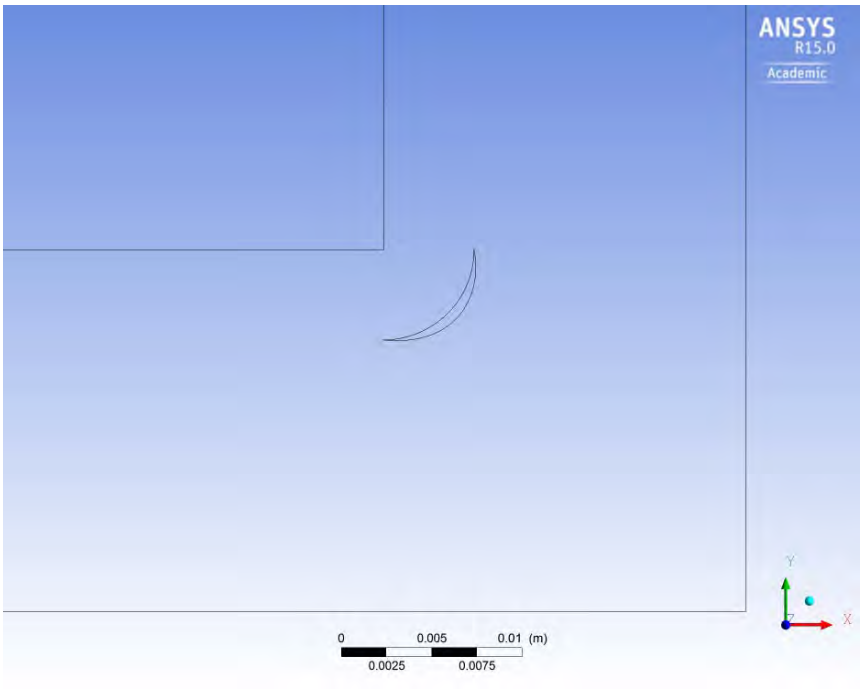

Figure 21. Profile view of one vane placed in upper left corner of 90^{o} bend configuration for D^{*} = 0.04, c^{*} = 0.18, r^{*} = 0.2, t^{*} = 0.07.

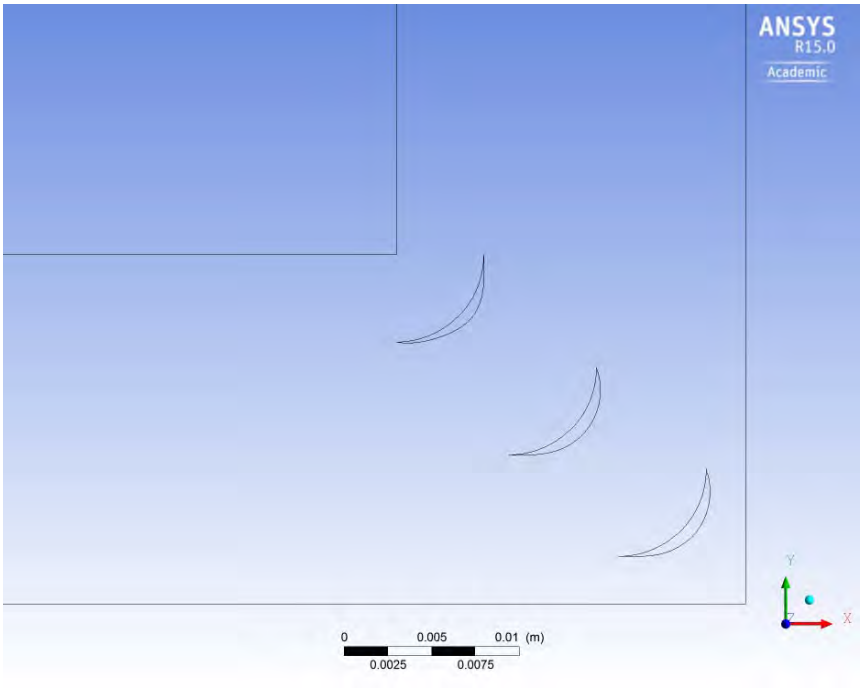

Figure 22. Profile view of three smaller vane configuration for D^{*} = 0.04, c^{*} = 0.18, r^{*} = 0.2, t^{*} = 0.07. Note: Multiple small vanes have been used in rounded ducts.

What the plotted values in Figure 17 shows are the drastic decrease in pressure drop over the vane for the varying vane configurations. Table 3 (below) compared the non-dimensional pressure drop of the single, centrally placed vane against the no vane configuration.

$\Delta P^* (\Delta P/\rho U^2)$ [1]		% Reduction from no vane to 1 vane
No vane	1 Vane	
1.364	0.524	61.6%
1.263	0.510	59.7%
1.347	0.516	61.7%
1.336	0.515	61.5%
1.495	0.517	65.4%
1.434	0.622	56.6%
1.390	0.663	52.3%
1.358	0.662	51.2%

Table 3. Non-dimensional pressure drop values and percentage reduction between single vane and no vane configurations.

When the pressure drop values for a single vane and no vane configuration are compared, as shown in Table 3, a decrease in pressure drop by 50–60% was observed. This drop in backpressure proved to be a significant result and demonstrated the great effectiveness that a simple turning vane has on the flow through a sharp-cornered bend. The application of the results found over the course of the research conducted in this thesis will greatly aid future work in WHR device placement and will provide a basis from which accurate pressure drop measurements can be recorded.

The significant drop in backpressure demonstrated in Figure 17 and in Table 3 show computationally calculated results for expected pressure drop in a real system. Moving forward with the application of this result will play a major role in increasing fuel economy, thus saving costs on the front end of operating a generator or an engine.

2. Plotted Results for ΔP^{**}

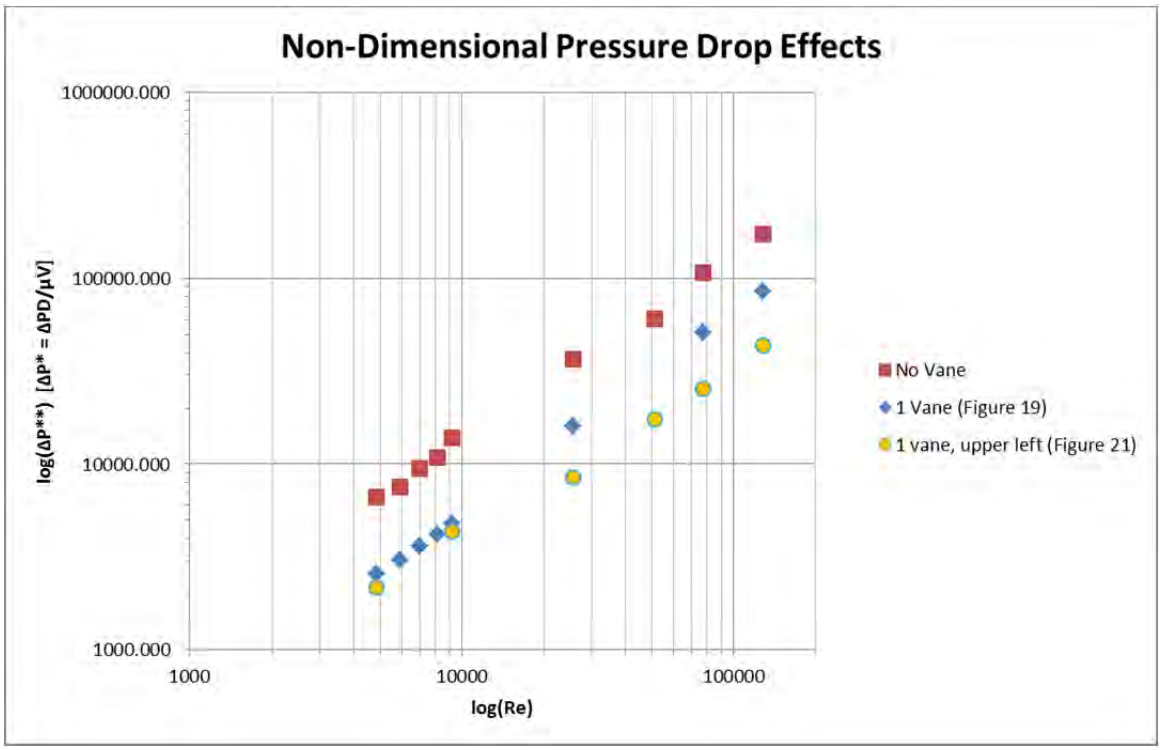

Figure 23. Non-dimensional pressure drop values for ΔP^{**} in an exhaust duct with a 90^{o} bend for $D^{*} = 0.04$.

The plot of ΔP^{**} shows plotted values of the pressure drop for three configurations: no vane, 1 vane located in the center of the bend (refer to Figure 19) and 1 vane located in the upper left corner of the bend (refer to Figure 21). The three-vane (Figure 22) and rotated vane (Figure 20) were omitted in order to more clearly see the effects of the vane placed in the upper left corner. The results in Figure 23 are significant in several ways. First, a noticeable pressure drop decrease is again noted from the no

vane configuration to the one-vane configurations. Second, there is an additional decrease of 10–15% in pressure drop from one vane to one vane placed in the upper left corner of the bend for $Re>2x10^4$. Third, a linear relationship is shown between pressure drop and Reynolds number.

The observed linear relationship between pressure drop and Reynolds number was a significant result. What this result proved is that as Reynolds increased, pressure drop increased proportionally. This relationship can be explained by the proportionality between Nusselt number and Reynolds number, which is used in heat transfer problems:

$$Nu \propto \mathrm{Re}^{a}\,\mathrm{Pr}^{b} \tag{24}$$

As Reynolds number increases and the flow becomes turbulent, $\mathrm{Pr} \approx 1$ and this term reduces the relationship in Equation 24 to the following:

$$Nu \propto \mathrm{Re}^{a} \tag{25}$$

A linear correlation exists when Nusselt and Reynolds numbers are plotted on a log-log plot. Shown in Figure 23 is a log-log plot of pressure drop and Reynolds number; from the results gathered by CFD modeling it is reasonable to accept that there exists a proportional relationship between pressure drop and Nusselt number. This proportionality will prove to be crucial in determining proper WHR device placement, as well as for measuring IR signature and overall heat transfer coefficients, which need to be predicted as accurately as possible in order to extract the most energy as possible from the exhaust gas flow.

Another key aspect in Figure 23 is the jump in the pressure drop when $Re > 10^4$. Both one-vane configurations follow nearly the same linear approximation for $Re < 10^4$, however once the flow evolved past $Re = 10^4$ a perceptible decrease in the pressure drop for the vane located in the upper left corner of the bend was observed. As shown in Table 1, the operating parameters for both the USMC GENSET and the USN LM2500 are above the $Re = 10^4$ range and thus having a vane placement closer to the corner where flow will initially shift its momentum would be more beneficial than a vane placed centrally in the bend.

$\Delta P^* (\Delta P/\rho U^2)$ [1]		% Reduction from no vane to 1 vane
No vane	1 Vane Upper Left Corner	
1.364	0.472	68.4%
1.495	0.442	67.6%
1.434	0.329	77.1%
1.182	0.340	77.3%
1.390	0.333	76.0%

Table 4. Non-dimensional pressure drop values and percentage reduction between a single vane in the upper left corner of the bend and no vane configurations. Refer to Figure 21 for geometry of 1 vane in upper left corner.

The data accumulated in Table 4 substantiates the data plotted in Figure 23 as well as the discussion noted above. Calculated decrease in pressure drop values ranged from 65–75% of the expected values for a 90^o bend without a turning vane. This is a 10–15% improvement over placing a turning vane in the center of the 90^o bend; significant enough to warrant discussion about proper vane placement within a bend for the sake of engine efficiency, fuel economy, and waste heat recovery.

3. Plotted Results for Recirculation Zone Size

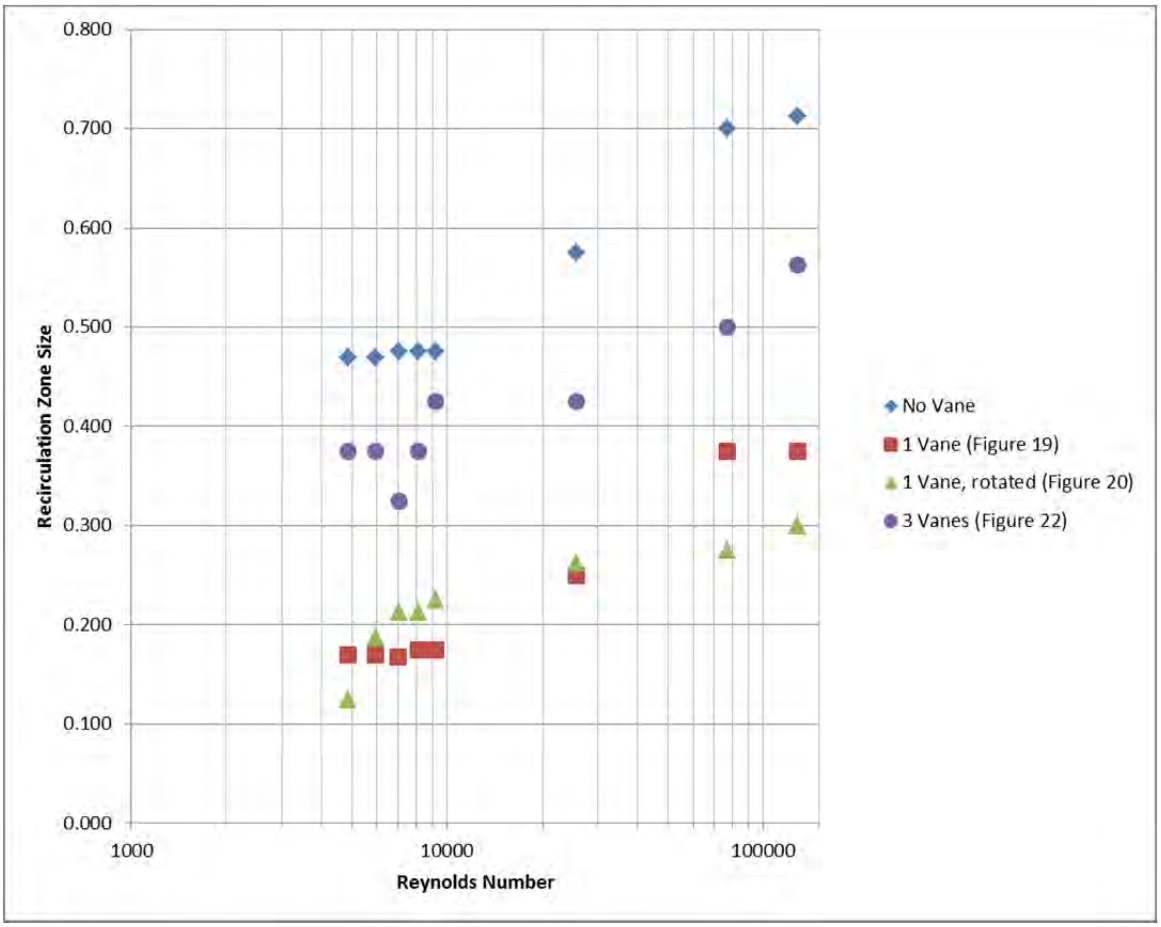

Figure 24. Non-dimensional recirculation zone size in an exhaust duct with 90^{o} bend for D^{*} = 0.04.

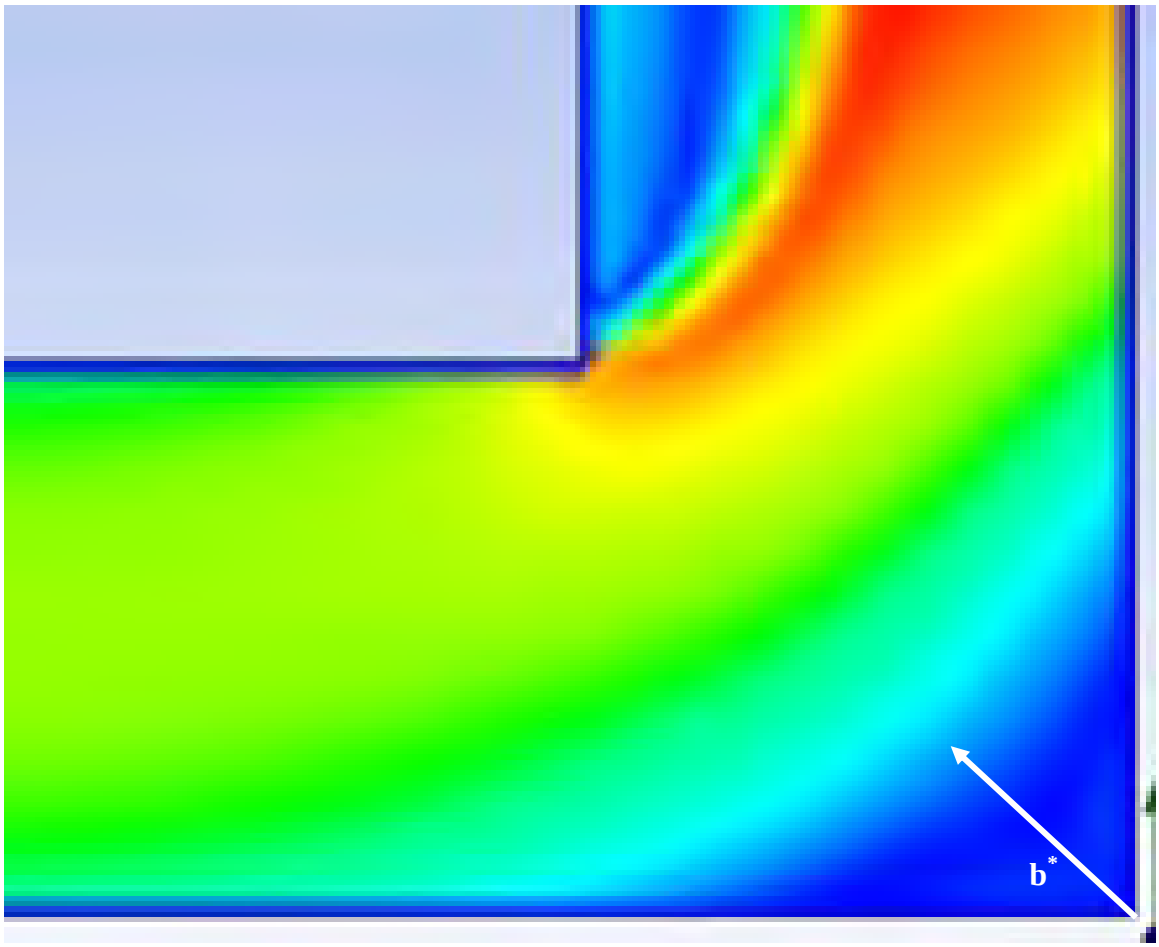

Figure 25. Non-dimensional primary recirculation zone size.

The non-dimensional recirculation data plotted in Figure 24 is relevant for several reasons (the non-dimensional recirculation zone size b^* is computed by measuring the distance from the outer corner at a 45^o angle until a u^* value of 0.4 is reached). First, it validated the assumption that in the 90^o bend without a turning vane the recirculation zone will be the largest. Second, it asserted the claim that a single turning vane will show drastic size reduction in the primary recirculation zone size, thereby decreasing soot accumulation. Third, it showed that an increase in the number of vanes is not entirely beneficial, and when compared to the results plotted for just a single vane, an increase in vane number actually increases the recirculation zone size. The relevance of this third argument is that in several sources referenced in this thesis the effect of the number of turning vanes on the recirculation zone size is not studied.

	b* Values			
Re	No Vane	1 Vane (Figure 19)	1 Vane, rotated (Figure 20)	3 Vanes Figure 22)
4900	0.469	0.170	0.125	0.375
6000	0.469	0.170	0.188	0.375
7000	0.475	0.168	0.213	0.325
8100	0.475	0.175	0.213	0.375
9200	0.475	0.175	0.225	0.425
25600	0.575	0.250	0.263	0.425
76800	0.700	0.375	0.275	0.500
128000	0.713	0.375	0.300	0.563

Table 5. Non-dimensional b^* values for various vane configurations for $D^* = 0.04$.

VII. CONCLUSION

The use of CFD software was a necessary tool used to study methods to reduce backpressure in an exhaust duct with a 90^{o} sharp-cornered bend. The effectiveness of placing a turning vane in the flow showed results that ranged from 50–75% reduction in backpressure across the bend. This significant reduction in backpressure will prove to be a significant factor in improving fuel economy of generators and engines used by the Marine Corps and Navy. Also, placement of a waste heat recovery device in the exhaust duct will increase backpressure, thus having ways to reduce this added backpressure must be found. In addition to reducing backpressure, turning vanes smoothed the turbulent flow as it encountered a shift in flow direction. This result will assist future developments in waste heat recovery device placement and will play a significant role in predicting and reducing infrared signature of the exhaust duct.

The objectives listed in Chapter I were accomplished, as shown in the chapters on model validation and in the results discussion. Specifically, with regard to creating a two-dimensional model that accurately represented real systems, this was accomplished using non-dimensional parameters and scaling said parameters to meet the dimensions of the model used. In terms of validating the model in both laminar and turbulent flow conditions, this was achieved and proved through various methods by comparing the CFD results to theoretical and expected values for the input conditions given. Finally, turning vane parameters were varied and their effects were studied; these results supported the claim that by translating a turning vane in a 90^{o} bend toward the area of initial momentum and flow direction change an improvement in pressure drop reduction will be observed.

With regard to the objectives listed in Chapter I, the following answers are given.

A two-dimensional model was created, satisfied the equations of continuity and momentum for an incompressible fluid using Cartesian coordinates. The model was validated for both laminar and turbulent regimes against expected fully developed laminar flow profiles for the laminar regime, and against expected Darcy friction factors

for the turbulent model. The model was varied for several parameters, to include turning vane location, turning vane number and turning vane orientation. The results from varying said parameters were collected, tabulated and plotted. These results were used to estimate pressure drop values compared to a ninety-degree sharp-angled exhaust duct bend.

The results of this thesis showed that the use of one centrally placed turning vane or three equally spaced turning vanes produced anywhere from 50–60% reduction in overall backpressure through the sharp-cornered 90^{o} exhaust duct bend. In contrast, a single turning vane placed near the inner corner of the same bend resulted in 65–75% reduction in backpressure. The effect of translating a single turning vane toward the inner corner of a sharp-angled exhaust duct bend showed great results, which will tie in to future developments and research in the energy harvesting programs. The recirculation zone size, which was very prevalent in the exhaust duct bend without any turning vanes, showed a dramatic decrease in size once a single turning vane configuration was considered. However, with addition of more turning vanes the recirculation zone did not decrease further in size; rather, it increased in size compared to the results from the single vane cases.

The application of this study toward the overall energy program coordinated between the Naval Postgraduate School and the U.S. Marine Corps Expeditionary Energy Office will provide a solid foundation for future endeavors in waste heat recovery and energy harvesting, as well as in infrared signature reduction. This research will also be applicable in the academic sense where follow-on work can be done in optimizing vane placement for a series of applications, and it also provides the groundwork for further studies in the effect of turning vane placement. The correlation between Nusselt number and pressure drop is an area of particular interest, and future studies will reveal significant correlations for application in current and future energy harvesting systems.

APPENDIX A. MODEL GEOMETRY

Created in SOLIDWORKS (mm, kg, s, K):
Inlet length: 1000 mm
Duct Height: 20 mm
Duct Width: 0.2 mm
Outlet length: 1000 mm
Boss extrude 0.2 mm (duct width)
Saved as parasolid, imported into ANSYS/CFX domain
Vane Dimensions
Chord Length: 14.14 mm
Turning Angle: 90^{o}

Model Meshing
Named boundaries:
Exhaust_In: This is the inlet to the 90-degree bend exhaust duct, located in the XY plane along the –X axis.
Exhaust_Out: this is the outlet to the 90-degree bend exhaust duct, located in the XY plane along the +Y axis.
Sym1: this is a symmetry boundary condition set up in the +Z direction to establish a semi-infinitely parallel plate in the +Z direction.
Sym2: this is a symmetry boundary condition set up in the -Z direction to establish a semi-infinitely parallel plate in the -Z direction.
Sym1, Sym2 combine to create two infinitely parallel plates, thus neglecting any wall effects in the +/-Z directions. This set up was used to evaluate a three-dimensional geometry in two dimensions.

Mesh
Method: Sweep Method
Free Face Mesh Type: Quad/Tri
Type: Number of Divisions: Sweep Number Divisions = 1
Relevance Center: Fine
Minimum Size: 0.2 mm
Maximum Face Size: 1.0 mm
Maximum Size: 1.0 mm
Curvature Normal Angle: 1.0^{o}
Growth Rate: Default (1.20)
Inflation
Use Automatic Inflation: All Faces in Chosen Named Selection
Named Selection: TurnVane
Default values for all other Inflation Settings

THIS PAGE INTENTIONALLY LEFT BLANK

APPENDIX B. MODEL SETUP

LAMINAR SETUP
Default Domain
Basic Settings
Location: Exhaust duct body
Domain Type: Fluid Domain
Coordinate Frame: Coord 0
Fluid and Particle Definitions: Fluid 1
Fluid 1
Option: Material Library
Material: Air at 25 C
Morphology: Continuous Fluid
Domain Models
Pressure
Reference Pressure: 1 [atm]
Buoyancy Model: Non Buoyant
Domain Motion: Stationary
Mesh Deformation: None
Fluid Models
Heat Transfer
Option: Isothermal
Turbulence
Option: None
Wall Function: N/A
Fluid Temperature: 25 [C]

Inlet
Basic Settings
Boundary Type: Inlet
Location: Exhaust_In
Boundary Details
Flow Regime: Subsonic
Mass and Momentum
Option: Mass Flow Rate
Mass Flow Rate: 1.85E-6 [kg/s] (for Re = 1000)
Flow Direction: Normal to Boundary Condition
Turbulence: None

Outlet
Basic Settings
Boundary Type: Outlet
Location: Exhaust_Out

Boundary Details
Flow Regime: Subsonic
Mass and Momentum
Option: Static Pressure
Relative Pressure: 0 [atm]

Sym1
Basic Settings
Boundary Type: Symmetry
Location: Sym1

Sym2
Basic Settings
Boundary Type: Symmetry
Location: Sym2

Solver Control
Basic Settings
Advection Scheme: High Resolution
Turbulence Numerics: First Order
Convergence Control
Min. Iterations: 1
Max. Iterations: 200
Fluid Timescale Control
Timescale Control: Auto Timescale
Length Scale Option: Conservative
Timescale Factor: 1.0
Convergence Criteria
Residual Type: RMS
Residual Target: 1E-6
Equation Class Settings
Equation Class: Continuity
Advanced Options
Dynamic Model Control
Global Dynamic Model Control

Air at 25 C
Basic Settings
Option: Pure Substance
Material Group: Air Data, Constant Property Gases
Material Description: Air at 25 C and 1 atm (dry)
Thermodynamic State: Gas
Material Properties
Option: General Material
Thermodynamic Properties

Equation of State
Option: Value
Molar Mass: 28.96 [kg $kmol^{-1}$]
Density: 1.185 [kg m^{-3}]
Specific Heat Capacity
Option: Value
Specific Heat Capacity: 1.0044E3 [J kg^{-1} K^{-1}]
Reference State
Option: Specified Point
Ref. Temperature: 25 [C]
Reference Pressure: 1 [atm]
Reference Specific Enthalpy
Ref. Spec. Enthalpy: 0 [J/kg]
Reference Specific Entropy
Ref. Spec. Entropy: 0 [J/kg/K]
Transport Properties
Dynamic Viscosity
Option: Value
Dynamic Viscosity: 1.831E-5 [kg m^{-1} s^{-1}]
Thermal Conductivity
Option: Value
Thermal Conductivity: 2.61E-2 [W m^{-1} K^{-1}]
Radiation Properties
Refractive Index
Option: Value
Refractive Index: 1.0 [m m^{-1}]
Scattering Coefficient
Option: Value
Scattering Coefficient: 0.0 [m^{-1}]
Buoyancy Properties
Option: Value
Thermal Expansivity: 0.003356 [K^{-1}]
Electromagnetic Properties: None

TURBULENT SETUP
All input conditions for turbulent models are similar to the laminar setup, with the exception of turbulence intensity, Re scaling and turbulence models that were selected appropriately below:
Default Domain
Fluid Models
Heat Transfer
Option: Isothermal
Turbulence
Option: k-Epsilon
Wall Function: Scalable

Inlet
Boundary Details
Turbulence: Medium (Intensity = 5%)

Note: A change in turbulence intensity from 3–10% changed pressure drop by less than 5% and had no significant effect on the flow patterns.

APPENDIX C. VELOCITY VECTOR PROFILE PLOTS FOR A 90^{O} EXHAUST BEND

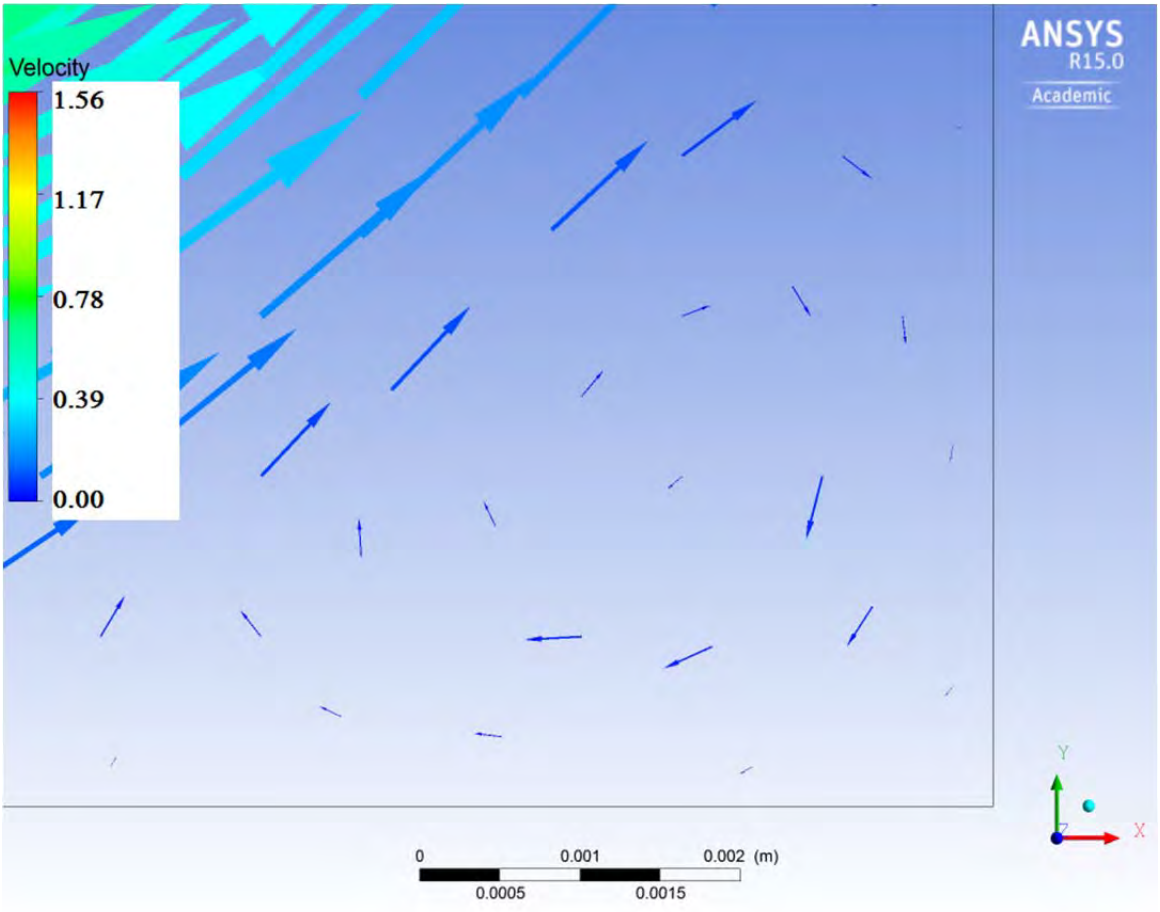

Figure 26. Non-dimensional velocity vectors in primary recirculation zone for Re = 76,800, D^{*} = 0.04, c^{*} = 0.35, r^{*} = 0.4, t^{*} = 0.07.

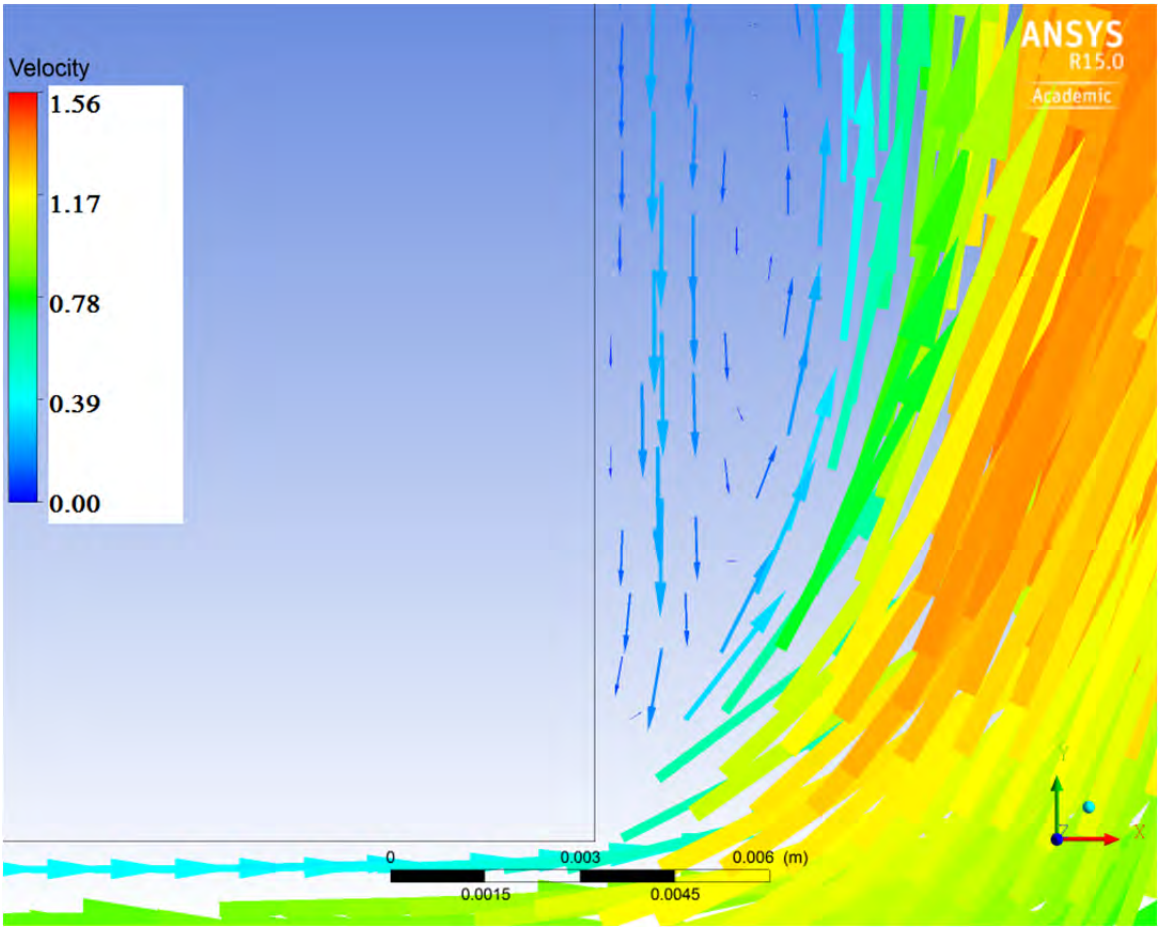

Figure 27. Non-dimensional velocity vectors in secondary recirculation zone for Re = 76,800, $D^* = 0.04$, $c^* = 0.35$, $r^* = 0.4$, $t^* = 0.07$.

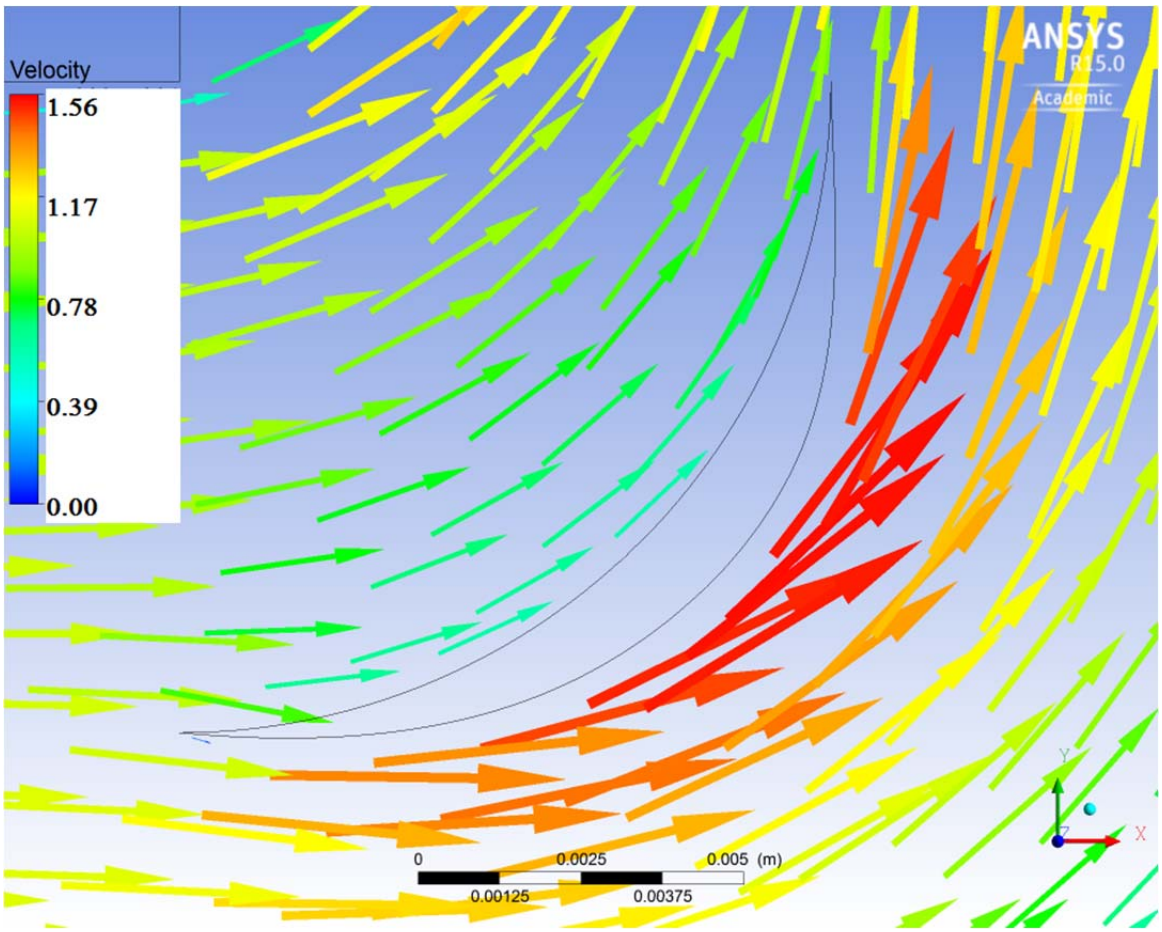

Figure 28. Non-dimensional velocity vectors along turning vane for Re = 76,800, $D^* = 0.04$, $c^* = 0.35$, $r^* = 0.4$, $t^* = 0.07$.

THIS PAGE INTENTIONALLY LEFT BLANK

LIST OF REFERENCES

Anand, K. D. (2006). *Fully developed pipe and channel flows.* Kharagpur: Indian Institute of Technology - Kharagpur.

Dudar, S. W. (2003). *Preliminary design study of an enhanced mixing eductor system for the LHA(R) gas turbine exhaust.* Naval Postgraduate School, Mechanical Engineering. Monterey: Naval Postgraduate School.

Hobson, G. (2013, November). Lecture 3 - Turbulence and its modeling. Monterey, CA , USA.

Idelchik, I. E. (1994). *Handbook of hydraulic resistance.* (M. O. Steinberg, Ed., & G. R. Malyavskaya, Trans.) Boca Raton: CRC Press.

Jafari, S., Rahnama, M., & Javaran, E. (2014). Simulation of turbulent duct flow by employing shear-improved smagorinsky model accompanied by forced generalized lattice boltzmann method. *International Journal of Numerical Methods for Heat & Fluid Flow* , 86-102.

Johnson, E. A., & Sathe, S. B. (1999). Patent No. 5914857. United States of America.

Kiijarvi, J. (2011, July 29). Darcy friction factor formulae in turbulent pipe flow. Lunowa Fluid Mechanics Paper , pp. 1-11.

Molki, A., et al. (2013). Measurement of fluid velocity development in laminar pipe flow using laser doppler velocimetry. *European Journal of Physics , 34* (5), 1127–1134.

Munson, B. R., Young, D. F., Okiishi, T. H., & Huebsch, W. W. (2009). *Fundamentals of fluid mechanics.* Hoboken: John Wiley & Sons, Inc.

Patankar, S. V. (1980). The turbulence-kinetic-energy equation. In S. V. Patankar, *Numerical heat transfer and fluid flow* (pp. 15–17). New York: Hemisphere Publishing Corporation.

Sathe, S. B., & Joshi, Y. (1992). Natural convection liquid cooling of a substrate-mounted protrusion in a square enclosure: a parametric study. *Journal of Heat Transfer* , 401–409.

Sathe, S., & Beale, M. (2013). Improving energy efficiency of diesel generators by optimizing exhaust duct designs. Naval Postgraduate School. Monterey: NPS.

Sathe, S., & Millsaps, K. (2014). WHRS program roadmap 2014–2020. Monterey: Naval Postgraduate School.

Schlichting, D. (1979). *Boundary-layer theory*. (D. Kestin, Trans.) New York: McGraw-Hill.

Singh, S. N., Seshadri, V., Singh, R. K., & Mishra, T. (2006). Flow characteristics of an annular gas turbine combustor model for reacting flows using CFD. *Journal of Scientific & Industrial Research* , 921–934.

Turns, S. R. (2012). *An introduction to combustion: concepts and application*. New Delhi: McGraw-Hill.

White, F. M. (2011). *Fluid mechanics.* New York: McGraw-Hill.

White, F. M. (2006). *Viscous fluid flow.* Boston: McGraw-Hill.

INITIAL DISTRIBUTION LIST

1. Defense Technical Information Center
   Ft. Belvoir, Virginia

2. Dudley Knox Library
   Naval Postgraduate School
   Monterey, California